Automatic Recognition of Space-Time Constellations by Learning on the Grassmann Manifold

Yuqing Du, Guangxu Zhu, Jiayao Zhang, and Kaibin Huang

Abstract

Recent breakthroughs in machine learning especially artificial intelligence shift the paradigm of wireless communication towards *intelligence radios*. One of their core operations is *automatic modulation recognition* (AMR). Existing research focuses on coherent modulation schemes such as QAM, PSK and FSK. The AMR of (non-coherent) space-time modulation remains an uncharted area despite its wide deployment in modern *multiple-input-multiple-output* (MIMO) systems. The scheme using a so called Grassmann constellation (comprising unitary matrices) enables rate-enhancement using multi-antennas and blind detection. In this work, we propose an AMR approach for Grassmann constellation based on data clustering, which differs from traditional AMR based on classification using a modulation database. The approach allows algorithms for clustering on the Grassmann manifold (or the Grassmannian), such as *Grassmann K-means* and *depth-first search* (DFS), originally developed for computer vision to be applied to AMR. We further develop an analytical framework for studying and designing these algorithms in the context of AMR. First, the *maximum-likelihood* (ML) Grassmann constellation detection is proved to be equivalent to clustering on the Grassmannian. Thereby, a well-known machine-learning result that was originally established only for the Euclidean space is rediscovered for the Grassmannian. Next, despite a rich literature on algorithmic design, theoretical analysis of data clustering is largely overlooked due to the lack of tractable techniques. We tackle the challenge by introducing probabilistic metrics for measuring the inter-cluster separability and intra-cluster connectivity of received space-time symbols and deriving them using tools from differential geometry and Grassmannian packing. The results provide useful insights into the effects of various parameters ranging from the signal-to-noise ratio to constellation size, facilitating algorithmic design.

Y. Du, G. Zhu, and K. Huang are with the Dept. of Electrical and Electronic Engineering and J. Zhang the Dept. of Computer Science, both at The University of Hong Kong, Hong Kong. Corresponding author: K. Huang (Email: huangkb@eee.hku.hk).

I. INTRODUCTION

Recent breakthroughs in machine learning has motivated researchers to apply the technology to the design of *intelligent radios* for automating communication systems so as to simplify their architectures or improve their performance. For instance, statistical learning has been used to merge channel estimation and data detection [1]–[3]. Moreover, it is also believed that radios with artificial intelligence can solve the long-standing challenge of spectrum scarcity [4]. Recent research trends in intelligent radios led to the revival of the classic areas of *cognitive radios* and *software defined radios* (SDR) [5] focusing on leveraging machine learning to attain a higher level of intelligence. In the areas of SDR or intelligent receivers, one important problem is *automatic modulation recognition* (AMR), where a receiver blindly detects the modulation type and order of the received signals. This problem is challenging due to many unknown parameters at the receiver such as the signal power, carrier frequency-and-phase offsets, and timing as well as channel hostility. In the last two decades, extensive research has been conducted on AMR for *linear* and *coherent* modulation schemes (such as BPSK, QPSK, and QAM) and frequency-shift keying [6], [7]. Interestingly, there exists little AMR technique for *nonlinear* and *non-coherent* space-time modulation (or called Grassmann modulation) despite the extensive deployment in *multiple-input-multiple-output* (MIMO) systems. Grassmann modulation has emerged to be a promising solution for low-latency machine-type communication as it enables blind detection without *channel state information* (CSI) and high data rates [8], [9]. This motivates the current work on filling the void of the area by developing a novel AMR approach for Grassmann modulation, which will find applications in next-generation multi-antenna intelligent radios.

A. Related Work and Motivation

1) Grassmann Modulation: Developed for MIMO systems, the modulation scheme features a constellation consisting a set of subspace matrices embedded in the space-time signal space. Mathematically, the matrices are points on a Grassmann manifold, giving the name *Grassmann constellation*. The idea of Grassmann modulation was originally proposed in [8], [10] for achieving a linear growth of data rate with respect to the array sizes and the feature of blind symbol detection without CSI. The feature results from the invariance of a Grassmann modulated symbol (an orthonormal matrix) to MIMO channel rotation, which gives the technology an alternative name of *non-coherent MIMO*. Extensive research in this area focuses on designing practical

Grassmann constellations including Fourier based [10] and hierarchical designs [11] for efficient constellation generation, differential modulation for coping with fast fading [8], [12], and error probability minimization [13]. From the information-theoretic perspective, the capacity of a MIMO channel with Grassmann modulation was studied in [14]. A key finding is that the capacity maximizing constellation is a solution of subspace packing on the Grassmannian.

Recent years have seen the resurgence of research interests on developing Grassmann modulation for next-generation wireless systems. The main reason is that its CSI-free feature makes it a promising solution for tackling the key challenges of reducing CSI overhead [15] and latency as faced by many next-generation technologies including massive MIMO using large-scale arrays [16], full-duplex relaying [17], and ultra-fast short-packet machine type communications [9]. In view of its applications in future systems, it is thus important to consider Grassmann modulation in intelligent receiver design.

2) Automatic Modulation Recognition: The principle design approach adopted in existing AMR algorithms is *classification* that maps the received signal to an element of a modulation database combining different modulation types and orders [6]. The algorithms can be separated into two groups based on two typical mapping criteria, namely *likelihood function* and *feature distance* [7]. In the presence of *additive white Gaussian noise* (AWGN) and given a set of signal samples, a likelihood based algorithm typically computes a likelihood function for each modulation scheme in the database and then selects the most likely scheme used for modulating the signal (see e.g., [18], [19]). Though operating in a similar way, a feature-based algorithm instead computes the feature vector of a modulated signal based on its distribution cumulants and then measures its vector distance to each modulation scheme (see e.g., [20]).

For feature-based AMR, the signal features derived from cumulants are design choices and may not be optimal especially for channels more complex than the AWGN channels. This motivates researchers to apply machine learning to train the modulation classifiers for improving the AMR accuracy [21]–[23]. Specifically, in [21], a hierarchical AMR algorithm was proposed that integrates *genetic programming* (GP) and the *K-nearest-neighbour* algorithm, both of which are classic machine learning techniques. Furthermore, a *deep neural network* was applied in [22] to AMR. For transmission over a MIMO channel, the received signal mixes a number of spatially multiplexed symbols, which increases the difficulty of AMR. It has been proposed in [23] that the challenge can be tackled using an *artificial intelligent network*.

Interestingly, though Grassmann modulation has been extensively studied and implemented in MIMO systems as discussed in the sequel, there exists no relevant AMR technique targeting the scheme. One possible reason is that existing designs cannot be straightforwardly extended to the Grassmann modulation due to its unique manifold structure. To be specific, existing AMR algorithms differentiate modulation schemes essentially by exploiting the statistical properties of a signal waveform in terms of phase, magnitude and frequency. This approach is suitable for signal reception using a single antenna but is insufficient for MIMO transmission. For a MIMO receiver, matrix based properties of array observations arise and it is important to exploit such properties in AMR. In particular, Grassmann modulated symbols are *orthonormal matrices* that are mathematically points on a Grassmannian embedded in the space-time signal space. How to exploit the unique manifold structure of Grassmann modulation in AMR remains an unexplored but important issue for its relevance to next-generation intelligent MIMO receivers.

From the perspective of intelligent radios, the classic AMR algorithms lack the desired intelligence and flexibility. To be specific, most algorithms involve a search over a modulation database comprising a set of combinations of modulation types and orders [6], [7]. It is impractical to include all possible combinations in the database as the required computing complexity is overwhelming. As the result, the recognition capability of a receiver is limited by the modulation database, which is a drawback of the classic AMR approach. The rapid advancement in unsupervised learning calls for the development of a modern intelligent AMR approach without the need of pre-specifying modulation types and orders.

B. Contributions

In this work, we attempt to fill a void in the AMR area by investigating automatic recognition of Grassmann modulation, referred to as *Grassmann AMR*. Specifically, the current work establishes a novel approach of Grassmann AMR based on data clustering on the Grassmannian via bridging the two areas of Grassmann AMR and unsupervised learning. Grassmann clustering algorithms were originally developed for computer vision (see e.g., [24]) and this is the first attempt on applying them to Grassmann AMR to the best of authors' knowledge. In the presence of channel noise, received Grassmann modulated symbols form clusters on the Grassmannian with corresponding codewords as their centers. Thus, it is a natural approach to apply manifold clustering techniques for AMR. Nevertheless, understanding its optimality and performance is

challenging but important for guiding algorithmic design. This motivates the current work whose main contributions are summarized as follows.

The first contribution of this work is to identify the connection between *maximum-likelihood (ML) detection* of Grassmann modulation and data clustering on the Grassmannian. To this end, we formulate the problem of ML constellation detection and consider the well-known *expectation-maximization* (EM) algorithm for solving the problem. The algorithm iterates between two steps, called the *E-step* and the *M-step*, till it converges. Under the assumption on high *signal-to-noise ratio* (SNR), it is proved that the E-step is equivalent to projecting a block of received symbols onto the Grassmann manifold and clustering the projections using a given initial or updated Grassmann constellation. On the other hand, it is further proved that the M-step is equivalent to inferring the Grassmann constellation via computing the centroids of the clusters of projected symbols. Combining the two equivalent steps is in fact the well-known *Grassmann K-means* algorithm in computer vision [24]. The connection establishes the optimality of the proposed low-complexity AMR approach. From the perspective of learning, the result represents a significant finding that the well-known connection between ML detection and data clustering originally known only for the linear Euclidean space [25] also holds on the non-linear Grassmannian.

The second contribution is to analyze the performance of the proposed approach of Grassmann constellation detection by data clustering. The developed framework not only yields theoretic insights useful for designing Grassmann AMR, but also fills the void of the data-clustering area that lacks tractable performance analysis [24], [25]. Specifically, we consider the K-means and *depth-first search* (DFS) algorithms for constellation detection with and without prior knowledge of constellation size, respectively. The performance of both algorithms depends on the separability of clusters in the dataset (the set of received symbols) and furthermore that of DFS requires the intra-cluster connectivity. To measure these dataset characteristics, suitable probabilistic metrics are defined and analyzed by developing novel techniques such as "Grassmannian bin packing" (see Fig. 3) for analyzing intra-cluster connectivity. These techniques leverage results from differential geometry and subspace packing [26]. The derived results quantify the effects of various parameters on the detection performance, such as the SNR, constellation and dataset sizes, space-time dimension, and the DFS threshold.

The last contribution of the work addresses the issue of how to embed a symbol-and-bit

mapping in a Grassmann constellation so as to enable a receiver to detect bits following the blind symbol-and-constellation detection. A simple method is proposed that assigns ordered bit sequences to constellation codewords following the order of their subspace distances to a reference matrix, which is designed to be a truncated Fourier matrix.

II. MATHEMATICAL PRELIMINARIES

To facilitate the subsequent exposition, several basic concepts and definitions related to Grassmann manifolds are introduced in this section.

A. Stiefel and Grassmann Manifolds

The (n, m) Stiefel manifold is the set of all n-by-m orthonormal matrices for $1 \leq m \leq n$, denoted by $\mathcal{T}_{n,m}$. Mathematically, the Stiefel manifold can be defined as follows:

$$\mathcal{T}_{n,m} = \{\mathbf{\Psi} \in \mathbb{C}^{n \times m} : \mathbf{\Psi}^H \mathbf{\Psi} = \mathbf{I}_m\}. \tag{1}$$

On the other hand, the (n, m) Grassmann manifold is a set of all m-dimensional subspaces in $\mathbb{C}^n$, denoted by $\mathcal{G}_{n,m}$. The manifold can be seen as the *quotient space* of $\mathcal{T}_{n,m}$. To be specific, a point on the Grassmann manifold corresponds to a class of n-by-m orthonormal matrices on the Stiefel manifold that span the same column subspace defined by the point. Choose an arbitrary matrix $\mathbf{\Upsilon}$ from this class, called a *generator*. Then the class, denoted as $[\mathbf{\Upsilon}]$, can be mathematically written as

$$[\mathbf{\Upsilon}] = \{\mathbf{\Upsilon}\mathbf{Q} : \mathbf{Q} \in \mathcal{O}_m\}. \tag{2}$$

where $\mathcal{O}_m$ denotes the group of $m \times m$ unitary matrices. The said relation between the Grassmannian $\mathcal{G}_{n,m}$ and the Stiefel $\mathcal{T}_{n,m}$ is typically represented by $\mathcal{G}_{n,m} = \mathcal{T}_{n,m}/\mathcal{O}_m$. Based on this relation and the definition of the class $[\mathbf{\Upsilon}]$ in (2), a Grassmann point mapped to this class can be then represented by the generator $\mathbf{\Upsilon}$ for ease of notation.

B. Tangent and Normal Spaces of Grassmann Manifold

To perform differential calculus on a manifold, one needs to specify its tangent and normal spaces. As illustrated in Fig. 1, for each point $\mathbf{\Upsilon}$ on the Grassmann manifold, there exists a *tangent space*, referred to the hyperplane tangent to the manifold at $\mathbf{\Upsilon}$ and having the same dimensions as that of the manifold. For any vector $\mathbf{\Delta}$ in the tangent space, it satisfies $\mathbf{\Upsilon}^H \mathbf{\Delta} = \mathbf{0}$. A *normal space* with respect to a given tangent space is defined to be the orthogonal complement of the latter. For each vector $\mathbf{N}$ in a normal space, it can be represented as $\mathbf{N} = \mathbf{\Upsilon}\mathbf{S}$, where $\mathbf{\Upsilon}$ is the point of tangency on the Grassmann manifold and $\mathbf{S}$ is some m-by-m symmetric matrix.
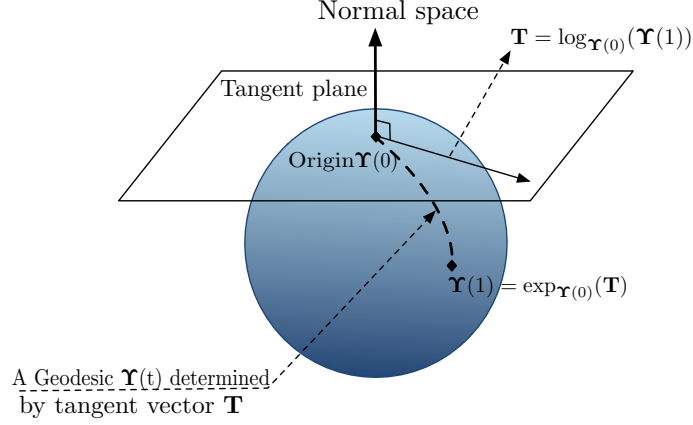
Figure 1. A Grassmann manifold and related subspaces and mappings.

C. Geodesics on Grassmann Manifold

Roughly speaking, a geodesic is the shortest curve linking two points on a Grassmannian as illustrated in Fig. 1. By representing the geodesic as a function $\boldsymbol{\Upsilon}(t)$ with $|t| \leq 1$, its two end points are $\boldsymbol{\Upsilon}(0)$ and $\boldsymbol{\Upsilon}(1)$. An important property of geodesics on a Grassmannian is given as follows.

Lemma 1 ([27]). For any geodesic $\boldsymbol{\Upsilon}(t)$ on a Grassmannian, it must satisfy the following equation:

$$\ddot{\boldsymbol{\Upsilon}} + \boldsymbol{\Upsilon}(t)(\dot{\boldsymbol{\Upsilon}}^H \dot{\boldsymbol{\Upsilon}}) = 0, \tag{3}$$

where $\dot{\boldsymbol{\Upsilon}} = d\boldsymbol{\Upsilon}(t)/dt$ is the *velocity vector* and $\ddot{\boldsymbol{\Upsilon}} = d^2\boldsymbol{\Upsilon}(t)/dt^2$ is the *acceleration vector*. The vectors $\dot{\boldsymbol{\Upsilon}}$ and $\ddot{\boldsymbol{\Upsilon}}$ lie in the tangent and normal space of the manifold, respectively.

D. Exponential and Logarithm Mappings

Definition 1 (Exponential Mapping [27]). As illustrated in Fig. 1, The exponential mapping, denoted by $\exp_{\boldsymbol{\Upsilon}(0)}(t\mathbf{T}) = \boldsymbol{\Upsilon}(t)$ with $|t| \leq 1$, is a one-to-one mapping from a velocity vector $t\mathbf{T} = t\dot{\boldsymbol{\Upsilon}}(0)$ in the tangent plane with the tangency at the point $\boldsymbol{\Upsilon}(0)$ to a point $\boldsymbol{\Upsilon}(t)$ on the Grassmannian. Mathematically, by denoting $\boldsymbol{\Upsilon}(0)$ as $\boldsymbol{\Upsilon}_0$ and decomposing $\mathbf{T}$ by *singular-value decomposition* (SVD) as $\mathbf{T} = \mathbf{U}\boldsymbol{\Sigma}\mathbf{V}^H$, the exponential mapping can be computed as

$$\exp_{\boldsymbol{\Upsilon}_0}(\mathbf{T}) = (\boldsymbol{\Upsilon}_0\mathbf{V} \quad \mathbf{U}) \begin{pmatrix} \cos\boldsymbol{\Sigma} \\ \sin\boldsymbol{\Sigma} \end{pmatrix} \mathbf{V}^H. \tag{4}$$

Definition 2 (Logarithm Mapping [27]). The logarithm mapping, denoted as $\log_{\boldsymbol{\Upsilon}(0)} \boldsymbol{\Upsilon}(t) = t\mathbf{T}$ with $|t| \leq 1$, is the *inverse exponential mapping* and maps a point on the Grassmann manifold

back to the corresponding velocity vector. Mathematically, given two points $\mathbf{A}$ and $\mathbf{B}$ on the Grassmann manifold, the logarithm mapping that generates a velocity vector $\mathbf{T}$ pointing from $\mathbf{A}$ to $\mathbf{B}$ can be computed as

$$\log_{\mathbf{A}} \mathbf{B} = \mathbf{T} = \mathbf{U\Sigma V}^H, \tag{5}$$

where the SVD components $\mathbf{U}$, $\mathbf{V}$ and $\mathbf{\Sigma}$ can be obtained via the *cosine-sine decomposition*:

$$\begin{pmatrix} \mathbf{V}(\cos \mathbf{\Sigma})\mathbf{V}^H \\ \mathbf{U}(\sin \mathbf{\Sigma})\mathbf{V}^H \end{pmatrix} = \begin{pmatrix} \mathbf{A}^H \mathbf{B} \\ (\mathbf{I} - \mathbf{A}\mathbf{A}^H)\mathbf{B} \end{pmatrix}. \tag{6}$$

III. SYSTEM MODEL

Consider a point-to-point MIMO system comprising a pair of multi-antenna transmitter and receiver. The numbers of transmit and receive antennas are denoted as N_t and N_r, respectively. It is assumed that N_r is larger than N_t so that the receiver can observe the space-time symbols. Time is slotted. Each space-time symbol occupies T slots. The block-fading channel model is adopted, where the channel coefficients remain unchanged within a symbol duration and change independently over different durations. The $N_t \times N_r$ MIMO channel matrix $\mathbf{H}$ comprises *independent and identically distributed* (i.i.d.) $\mathcal{CN}(0,1)$ coefficients. Consider the i-th symbol duration in a block of N space-time symbols. Let $\mathbf{X}^{(i)}$ denote the transmitted space-time symbol that is a $T \times N_t$ matrix, $\mathbf{H}^{(i)}$ the channel matrix, and $\mathbf{Y}^{(i)}$ the $T \times N_r$ received symbol. For ease of notation, following [10], [11], the baseband input-output relationship of the system can be written as

$$\mathbf{Y}^{(i)} = \mathbf{X}^{(i)}\mathbf{H}^{(i)} + \sqrt{\frac{N_t}{\rho T}}\mathbf{W}^{(i)}, \; i = 1, 2, \cdots, N, \tag{7}$$

where ρ represents the transmit SNR and $\mathbf{W}^{(i)} \in \mathbb{C}^{T \times N_r}$ the AWGN comprising i.i.d. $\mathcal{CN}(0,1)$ elements.

Assumption 1 (Receiver Knowledge). The receiver has no knowledge of the Grassmann constellation used by the transmitter. However, the receiver has information on the size of the transmit array, N_t, the symbol duration T and symbol boundaries so as to receive the symbol block $\{\mathbf{Y}^{(i)}\}$ in (7).[1]

---

[1]Under the assumption of $N_r \geq N_t$, N_t can be estimated by observing the ranks of received data symbols. For receiver synchronization, the symbol duration and boundaries can be estimated using standard methods in the literature (see e.g., [6]).

Transmitted symbols $\{\mathbf{X}^{(i)}\}$ are modulated using a Grassmann constellation codebook, denoted as $\mathcal{F}$. On the other hand, the codebook detected by the receiver is denoted as $\hat{\mathcal{F}}$. To combat fading and enable non-coherent detection without CSI, the $T \times N_t$ modulated symbols are designed to be "tall" matrices with $T \geq N_t$. Consequently, information is embedded in the column space of each symbol. It is important to note that given tall symbol matrices, propagation over the MIMO channel changes only the symbol's row space but not its column space. Therefore, the symbols $\{\mathbf{X}^{(i)}\}$ can be detected at the receiver by computing the column spaces of received symbols $\{\mathbf{Y}^{(i)}\}$ without requiring CSI [8], [10]. For consistency in matrix notation, let the Grassmann codebook $\mathcal{F}$ be a set of $T \times N_t$ tall orthonormal matrices, called *codewords*: $\mathcal{F} = \{\boldsymbol{\mu}_\ell\}$ with $\boldsymbol{\mu}_\ell \in \mathbb{O}^{T \times N_t}$, where $\mathbb{O}$ represents the group of orthonormal matrices.

From the perspective of communication performance, it is well known that it is desirable to maximize the pairwise distances between elements of the constellation $\mathcal{F}$. In other words, the optimal constellation design is related to the following problem of subspace packing [28], [29]:

$$\text{(Subspace Packing)} \quad \max_{\mathcal{F} \subset \mathcal{G}} \min_{\ell \neq n} d(\boldsymbol{\mu}_\ell, \boldsymbol{\mu}_n), \tag{8}$$

where $d(\cdot, \cdot)$ is a subspace distance metric. Among many others, two commonly used metrics are considered in this paper, namely *geodesic distance*, denoted as $d_g(\cdot, \cdot)$ and *Procrustes distance*, denoted as $d_p(\cdot, \cdot)$. Given two points $\boldsymbol{\Upsilon}$ and $\boldsymbol{\Upsilon}'$ on the Grassmannian, $d_g(\boldsymbol{\Upsilon}, \boldsymbol{\Upsilon}')$ measures the length of the geodesic and $d_p(\boldsymbol{\Upsilon}, \boldsymbol{\Upsilon}')$ the Euclidean distance between them:

$$d_g(\boldsymbol{\Upsilon}, \boldsymbol{\Upsilon}') = \| \log_{\boldsymbol{\Upsilon}}(\boldsymbol{\Upsilon}') \|_F, \tag{9}$$

$$d_p^2(\boldsymbol{\Upsilon}, \boldsymbol{\Upsilon}') = N_t - \text{tr}\left\{ \boldsymbol{\Upsilon}\boldsymbol{\Upsilon}^H \boldsymbol{\Upsilon}'(\boldsymbol{\Upsilon}')^H \right\}, \tag{10}$$

where $\log_{\boldsymbol{\Upsilon}}(\boldsymbol{\Upsilon}')$ is the logarithm mapping defined in (5) and N_t denotes the dimension of the Grassmannian. Finding the optimal constellation by subspace packing is in general intractable and typically relies on numerical computation [28]. However, the computed constellation is not unique, which further motivates the assumption of unknown constellation at the receiver and the need of AMR.

IV. PROBLEM FORMULATION

In this section, we first formulate the problem of ML symbol detection and then build on it to formulate the problem of ML Grassmann constellation detection.

A. Maximum-Likelihood Symbol Detection

Consider the communication model in (7) and the assumed Gaussian distributions of channel and noise. Given the transmitted symbols $\{\mathbf{X}^{(i)}\}$ and no CSI, the received symbols $\{\mathbf{Y}^{(i)}\}$ are i.i.d. complex Gaussian random matrices whose conditional distribution is $\mathbf{Y}^{(i)}|\mathbf{X}^{(i)} \sim \mathcal{CN}\left(\mathbf{0}, \mathbf{X}^{(i)}(\mathbf{X}^{(i)})^H + \frac{N_t}{\rho T}\mathbf{I}_T\right)$. Specifically, the distribution is given by [11]

$$p(\mathbf{Y}^{(i)}|\mathbf{X}^{(i)}) = \frac{\exp\left(-\frac{\rho T}{N_t}\mathrm{tr}\left((\mathbf{Y}^{(i)})^H(\mathbf{I}_T - \frac{1}{1+N_t/\rho T}\mathbf{X}^{(i)}(\mathbf{X}^{(i)})^H)\mathbf{Y}^{(i)}\right)\right)}{(\pi N_t/\rho T)^{TN_t}(1 + \rho T/N_t)^{N_t N_r}}. \tag{11}$$

For the conventional case where the constellation codebook $\mathcal{F}^*$ is known at receiver, the problem of ML symbol detection can be mathematically formulated as (see e.g., [11])

$$\hat{\mathbf{X}}^{(i)} = \max_{\mathbf{X}^{(i)}\in\mathcal{F}^*} p(\mathbf{Y}^{(i)}|\mathbf{X}^{(i)}), \ \forall i. \tag{12}$$

Based on (11), an equivalent problem is

$$\hat{\mathbf{X}}^{(i)} = \arg\max_{\mathbf{X}^{(i)}\in\mathcal{F}^*} \mathrm{tr}\left\{(\mathbf{Y}^{(i)})^H\mathbf{X}^{(i)}(\mathbf{X}^{(i)})^H\mathbf{Y}^{(i)}\right\}, \ \forall i. \tag{13}$$

B. Maximum-Likelihood Constellation Detection

For the current case that the ground-true constellation $\mathcal{F}^*$ is unknown *a priori*, we need to first infer $\mathcal{F}^*$ from the block of received symbols $\mathbf{Y} = \{\mathbf{Y}^{(i)}\}_{i=1}^N$. To simplify exposition, even though $\mathcal{F}^*$ is unknown, its size, denoted as L, is assumed to be known at the receiver. The issue of unknown constellation size at the receiver is addressed in Sections VI-B. Then the ML problem formulation is

$$\hat{\mathcal{F}} = \arg\max_{\mathcal{F}} \log p(\mathbf{Y}|\mathcal{F}) = \arg\max_{\mathcal{F}} \sum_{i=1}^N \log p(\mathbf{Y}^{(i)}|\mathcal{F}). \tag{14}$$

The likelihood function $p(\mathbf{Y}^{(i)}|\mathcal{F})$ follows the *mixture of Gaussian* (MoG) model given by

$$p(\mathbf{Y}^{(i)}|\mathcal{F}) = \sum_\ell p(\mathbf{Y}^{(i)}|\mathbf{X}^{(i)} = \boldsymbol{\mu}_\ell, \mathcal{F})p(\mathbf{X}^{(i)} = \boldsymbol{\mu}_\ell|\mathcal{F}), \ \forall i. \tag{15}$$

To facilitate subsequent analysis, we introduce a new latent variable $\mathbf{Z} = [\mathbf{z}_1, \ldots, \mathbf{z}_N]$ where $\mathbf{z}_i = [z_{i,1}, z_{i,2}, \cdots, z_{i,L}]^T$ is a L-dimensional binary random vector indicating the index of codeword modulating the i-th transmitted symbol $\mathbf{X}^{(i)}$. For instance, if $\{\mathbf{X}^{(i)} = \boldsymbol{\mu}_\ell\}$, we have $z_{i,\ell} = 1$ with the remaining elements in $\mathbf{z}_i$ being zeros. Due to the equivalence between the two events $\{z_{i,\ell} = 1\}$ and $\{\mathbf{X}^{(i)} = \boldsymbol{\mu}_\ell\}$, the MoG model in (15) can be rewritten as

$$p(\mathbf{Y}^{(i)}|\mathcal{F}) = \sum_\ell p(\mathbf{Y}^{(i)}|\mathbf{z}_{i,\ell} = 1, \mathcal{F})p(\mathbf{z}_{i,\ell} = 1|\mathcal{F}), \ \forall i. \tag{16}$$

By substituting (16) into (14), the problem of constellation detection is rewritten as

$$\hat{\mathcal{F}} = \arg\max_{\mathcal{F}} \sum_{i=1}^{N} \log \sum_{\ell} p(\mathbf{Y}^{(i)}|\mathbf{z}_{i,\ell} = 1, \mathcal{F})p(\mathbf{z}_{i,\ell} = 1|\mathcal{F}). \tag{17}$$

Directly solving this optimization problem is intractable due to the *non-convexity* of the objective function arising from the existence of the latent *random variable* (r.v.) $\mathbf{Z}$ (or equivalently the symbols $\{\mathbf{X}^{(i)}\}$). A commonly used approach for solving such a non-convex ML problem with latent variables is the EM algorithm as discussed in the following section.

V. GRASSMANN CONSTELLATION DETECTION: FROM EM TO DATA CLUSTERING

In this section, we consider the application of the well-known EM algorithm for solving the problem of ML constellation detection formulated in the preceding section. The main task of this section is to prove the equivalence between the EM algorithm and the proposed detection approach of data clustering on the Grassmannian.

A. Grassmann Constellation Detection by EM

1) Implementation of EM: Consider the problem of ML estimation of the codebook $\mathcal{F}$ based on the observation $\mathbf{Y}$ and given a latent variable $\mathbf{Z}$. The EM algorithm for solving the problem specified in (17) iterates between the two main steps [25]:

$$(\mathbf{E-step}) : \text{ Evaluate } \quad p(\mathbf{Z}|\mathbf{Y}, \hat{\mathcal{F}}) = \prod_{i=1}^{N} \prod_{\ell=1}^{L} r_{i,\ell}^{z_{i,\ell}}, \tag{18}$$

$$(\mathbf{M-step}) : \text{ Solve } \quad \hat{\mathcal{F}} = \arg\max_{\mathcal{F}} \mathbb{E}_{\mathbf{Z}}[\log p(\mathbf{Y}, \mathbf{Z}|\mathcal{F})], \tag{19}$$

where we define $r_{i,\ell} = p(z_{i,\ell} = 1|\mathbf{Y}^{(i)}, \hat{\mathcal{F}})$. For the E-step in (18), the posterior distribution of the latent variable $\mathbf{Z}$ is calculated using the current estimation of the codebook $\hat{\mathcal{F}}$, where the calculation involves evaluating the set of variables $\{r_{i,\ell}\}$. For the M-step in (19), the codebook $\hat{\mathcal{F}}$ is updated by maximizing the expectation of the complete-data log-likelihood, which can be evaluated using the posterior distribution updated in the E-step as follows:

$$\mathbb{E}_{\mathbf{Z}}[\log p(\mathbf{Y}, \mathbf{Z}|\mathcal{F})] = \sum_{\mathbf{Z}} p(\mathbf{Z}|\mathbf{Y}, \mathcal{F}) \log p(\mathbf{Y}, \mathbf{Z}|\mathcal{F}) \tag{20}$$

$$= \sum_{\mathbf{Z}} p(\mathbf{Z}|\mathbf{Y}, \mathcal{F}) \log \left(p(\mathbf{Y}|\mathbf{Z}, \mathcal{F})p(\mathbf{Z}) \right). \tag{21}$$

The specific expressions of the E-step and M-step can be derived as follows. For ease of notation, denote $\pi_{\ell} = p(z_{i,\ell} = 1)$. It follows that $p(\mathbf{Z}) = \prod_{i=1}^{N} \prod_{\ell=1}^{L} \pi_{\ell}^{z_{i,\ell}}$ and $p(\mathbf{Y}|\mathbf{Z}, \mathcal{F}) =$

$\prod_{i=1}^{N} \prod_{\ell=1}^{L} p(\mathbf{Y}^{(i)}|\mathbf{X}^{(i)} = \boldsymbol{\mu}_\ell, \mathcal{F})^{z_{i,\ell}}$. Substituting them into (21) and following the standard procedure in [25, Section 9.3], the E-step variables $\{r_{i,\ell}\}$ and $\mathbb{E}_{\mathbf{Z}}[\log p(\mathbf{Y}, \mathbf{Z}|\mathcal{F})]$ for the M-step are given by:

$$r_{i,\ell} = \frac{\pi_\ell p(\mathbf{Y}^{(i)}|\mathbf{X}^{(i)} = \hat{\boldsymbol{\mu}}_\ell, \hat{\mathcal{F}})}{\sum_{j=1}^{L} \pi_j p(\mathbf{Y}^{(i)}|\mathbf{X}^{(i)} = \hat{\boldsymbol{\mu}}_j, \hat{\mathcal{F}})}, \tag{22}$$

$$\mathbb{E}_{\mathbf{Z}}[\log p(\mathbf{Y}, \mathbf{Z}|\mathcal{F})] = \sum_{i=1}^{N} \sum_{\ell=1}^{L} r_{i,\ell}(\log \pi_\ell + \log p(\mathbf{Y}^{(i)}|\mathbf{X}^{(i)} = \boldsymbol{\mu}_\ell, \mathcal{F})). \tag{23}$$

Note that the probability $r_{i,\ell}$ can be interpreted as a *soft assignment* of the i-th received symbol $\mathbf{Y}^{(i)}$ to the ℓ-th codeword $\hat{\boldsymbol{\mu}}_\ell$. Moreover, given the estimated $\{r_{i,\ell}\}$ and using (11), one can show that maximizing (23) in the M-step is equivalent to maximizing $\sum_{i=1}^{N} \sum_{\ell=1}^{L} r_{i,\ell} \text{tr}\left\{(\mathbf{Y}^{(i)})^H \boldsymbol{\mu}_\ell \boldsymbol{\mu}_\ell^H \mathbf{Y}^{(i)}\right\}$. Thereby, the EM algorithm for Grassmann constellation detection can be implemented as:

$$(\mathbf{E-step}) : \text{Evaluate } \{r_{i,\ell}\} \text{ using (22).} \tag{24}$$

$$(\mathbf{M-step}) : \text{Solve } \hat{\mathcal{F}} = \arg\max_{\mathcal{F}} \sum_{i=1}^{N} \sum_{\ell=1}^{L} r_{i,\ell} \text{tr}\left\{(\mathbf{Y}^{(i)})^H \boldsymbol{\mu}_\ell \boldsymbol{\mu}_\ell^H \mathbf{Y}^{(i)}\right\}. \tag{25}$$

2) Difficulties of EM Implementation: The direct application of the EM algorithm faces two main difficulties described as follows.

- The optimization problem in the M-step in (25) is *non-convex* and thus difficult to solve. Specifically, the non-convexity is due to the maximimization of a convex object function under the constraints that the codewords (variables) $\{\boldsymbol{\mu}_\ell\}$ are subspace matrices or equivalently points on the Grassmannian.

- The convergence for implementing the EM algorithm based on the MoG model in (15) is potentially slow as the model involves Gaussian components with overlapping means (that are all zeros). As proved in [30], the convergence rate of the EM algorithm on a MoG model is faster if the Gaussian components are better separated.

To overcome these difficulties, we prove in the sequel the equivalence of the EM algorithm with the Grassmann K-means algorithm, a widely used clustering algorithm. The latter algorithm has a faster convergence rate and lower complexity due to the well-separated symbol clusters "seen" on the Grassmannian as revealed in Lemma 7 in the sequel and the discussion therein.

B. Asymptotic Equivalence between EM and Data Clustering

In this sub-section, we prove that the EM algorithm for Grassmann constellation detection as derived in the preceding section is asymptotic equivalent to data clustering on the Grassmannian when the transmit SNR is high and the dataset size N is sufficiently large. The result allows the replacement of the complex EM algorithm with the low-complexity clustering algorithms from machine learning.

1) From E-step to symbol detection: Consider the EM E-step in (24). First, substituting the conditional distribution of the received symbol $\mathbf{Y}^{(i)}$ in (11) into the soft assignments $\{r_{i,\ell}\}$ in (22) leads to the following result.

Lemma 2. (From Soft to Hard Assignments). For a high transmit SNR ($\rho \to \infty$), the soft assignments of received symbols, $\{r_{i,\ell}\}$, become *hard assignments* taking only binary values:

$$r_{i,\ell} \to \begin{cases} 1, & \ell = \arg\max_{j} \operatorname{tr}\left\{ (\mathbf{Y}^{(i)})^{H} \hat{\boldsymbol{\mu}}_{j} (\hat{\boldsymbol{\mu}}_{j})^{H} \mathbf{Y}^{(i)} \right\}; \\ 0, & \text{otherwise}, \end{cases} \tag{26}$$

where $\mathbf{Y}^{(i)}$ is the i-th received symbol and $\hat{\boldsymbol{\mu}}_{j}$ the j-th codeword in the estimated codebook $\hat{\mathcal{F}}$.

Next, we can show that the hard assignments of symbols to codewords in Lemma 2 are approximately based on the criterion of *shortest subspace distance*. To this end, define the i-th received Grassmann symbol $\boldsymbol{\Upsilon}^{(i)}$ as the dominant N_t dimensions of the left eigen-space of the received symbol $\mathbf{Y}^{(i)}$, which is its only SVD component containing information on the transmitted symbol. Specifically, consider the following SVD of $\mathbf{Y}^{(i)}$

$$\mathbf{Y}^{(i)} = \begin{bmatrix} \mathbf{U}_{Y}^{(i)} & \mathbf{U}_{W}^{(i)} \end{bmatrix} \begin{bmatrix} \boldsymbol{\Sigma}_{Y}^{(i)} & \mathbf{0} \\ \mathbf{0} & \boldsymbol{\Sigma}_{W}^{(i)} \end{bmatrix} \begin{bmatrix} (\mathbf{V}_{Y}^{(i)})^{H} \\ (\mathbf{V}_{W}^{(i)})^{H} \end{bmatrix}, \tag{27}$$

where the diagonal elements of $\boldsymbol{\Sigma}_{Y}^{(i)}$ and $\boldsymbol{\Sigma}_{W}^{(i)}$ are the $q = \min(N_r, T)$ singular-values $\sigma_1, \sigma_2, \cdots, \sigma_q$ arranged in the descending order, and $\mathbf{U}_{Y}^{(i)}$ and $(\mathbf{V}_{Y}^{(i)})^{H}$ are the dominant N_t dimensional left and right eigen-subspace, respectively. Then the Grassmann symbol (a tall matrix) is $\boldsymbol{\Upsilon}^{(i)} = \mathbf{U}_{Y}^{(i)}$.

Lemma 3. The hard assignment criteria in Lemma 2 can be bounded as follows:

$$\left(\sigma_{N_t}^{(i)} \right)^2 \left[N_t - d_p^2 \left(\boldsymbol{\Upsilon}^{(i)}, \hat{\boldsymbol{\mu}}_j \right) \right] \leq \operatorname{tr}\left\{ (\mathbf{Y}^{(i)})^{H} \hat{\boldsymbol{\mu}}_{j} (\hat{\boldsymbol{\mu}}_{j})^{H} \mathbf{Y}^{(i)} \right\} \tag{28}$$

$$\leq \left(\sigma_{1}^{(i)} \right)^2 \left[N_t - d_p^2 \left(\boldsymbol{\Upsilon}^{(i)}, \hat{\boldsymbol{\mu}}_j \right) \right], \tag{29}$$

where $\sigma_k^{(i)}$ denotes the k-th singular value of the received symbol $\mathbf{Y}^{(i)}$, and $d_p(\cdot, \cdot)$ is the Procrustes distance defined in (10).

The proof is presented in Appendix A. Approximating the hard assignment criteria in Lemma 2 by either the lower or the upper bound in Lemma 3 leads to the following hard-assignment based on the Procrustes distance:

$$r_{i,\ell} \rightarrow \begin{cases} 1, & \ell = \arg \min_j d_p^2 \left(\boldsymbol{\Upsilon}^{(i)}, \hat{\boldsymbol{\mu}}_j \right); \\ 0, & \text{otherwise}. \end{cases} \tag{30}$$

It follows that the E-step of the EM algorithm in (24) can be approximated by the computation of the assignment variables $\{r_{i,\ell}\}$ using (30). As a result, the E-step is equivalent to clustering the received symbols using the estimated codewords $\{\hat{\boldsymbol{\mu}}_j\}$ and the criteria of shortest Procrustes distance. Note that in the high SNR regime, one can infer from the system equation in (7) that the singular values of $\mathbf{Y}^{(i)}$ are approximately equal to those of the channel matrix $\mathbf{H}^{(i)}$. Thus, when the channel is well conditioned $\left(\sigma_{N_t}^{(i)} \approx \sigma_1^{(i)} \right)$, the approximation of the E-step by (30) is accurate.

2) From M-step to codeword optimization: Consider the EM M-step in (25). For a sufficiently high SNR and a sufficiently large dataset size, it is proved in the sequel that the M-step is equivalent to codeword optimization. Specifically, each estimated codeword in the constellation codebook is updated by computing the Grassmann *centroid*, which has the minimum sum subspace distances to the cluster of estimated Grassmann symbols associated with the codeword.

Consider a particular cluster of received symbols detected as the ℓ-th codeword in the E-step. Their indices can be grouped in the set $\mathcal{C}_\ell = \{i \mid r_{i,\ell} = 1\}$ with the assignments $\{r_{i,\ell}\}$ given in Lemma 2. The number of symbols in $\mathcal{C}_\ell$ is denoted as $N_\ell = |\mathcal{C}_\ell|$. Consider the M-step in (25). Using the definition of the index set $\mathcal{C}_\ell$, the M-step can be rewritten as

$$\hat{\mathcal{F}} = \arg \max_{\mathcal{F}} \sum_{\ell=1}^{L} \sum_{i \in \mathcal{C}_\ell} \text{tr} \left\{ (\mathbf{Y}^{(i)})^H \boldsymbol{\mu}_\ell \boldsymbol{\mu}_\ell^H \mathbf{Y}^{(i)} \right\}. \tag{31}$$

This is equivalent to optimizing the codewords as follows:

$$\hat{\boldsymbol{\mu}}_\ell = \arg \max_{\boldsymbol{\mu}_\ell \in \mathcal{G}} \sum_{i \in \mathcal{C}_\ell} \text{tr} \left\{ (\mathbf{Y}^{(i)})^H \boldsymbol{\mu}_\ell \boldsymbol{\mu}_\ell^H \mathbf{Y}^{(i)} \right\}, \quad \forall \ell. \tag{32}$$

Next, an asymptotic form of the above codeword optimization is obtained for the case of large dataset size. To this end, define the minimum (pairwise) distance of the constellation codebook

$\mathcal{F}$ as

$$d_{\min} = \min_{\substack{\boldsymbol{\mu}, \boldsymbol{\mu}' \in \mathcal{F} \\ \boldsymbol{\mu} \neq \boldsymbol{\mu}'}} d_p(\boldsymbol{\mu}, \boldsymbol{\mu}'). \tag{33}$$

Lemma 4. If the minimum distance of the codebook $\mathcal{F}$ is strictly positive and all codewords are transmitted with equal probabilities, as the symbol dataset size $N \to \infty$, the symbol cluster size $N_\ell \to \infty$ for all ℓ.

The proof is presented in Appendix B. Using the result and applying the law of large numbers, we can obtain the following important asymptotic form of the summation term in (32).

Lemma 5. As the dataset size grows ($N \to \infty$),

$$\sum_{i \in \mathcal{C}_\ell} \text{tr}\left\{ (\mathbf{Y}^{(i)})^H \boldsymbol{\mu}_\ell \boldsymbol{\mu}_\ell^H \mathbf{Y}^{(i)} \right\} \longrightarrow \sum_{i \in \mathcal{C}_\ell} \left[N_t - d_p^2 \left(\boldsymbol{\Upsilon}^{(i)}, \boldsymbol{\mu}_\ell \right) \right], \qquad \forall \ell. \tag{34}$$

The proof is provided in Appendix C. Substituting the result in Lemma 5 into (32) yields the following asymptotic form of the M-step in (25) in the case of high SNR and large dataset size:

$$\hat{\boldsymbol{\mu}}_\ell = \arg\min_{\boldsymbol{\mu}_\ell \in \mathcal{G}} \sum_{i \in \mathcal{C}_\ell} d_p^2 \left(\boldsymbol{\Upsilon}^{(i)}, \boldsymbol{\mu}_\ell \right), \quad \forall \ell. \tag{35}$$

In this form, the M-step updates each codeword by computing the Grassmann centroid of the cluster of Grassmann symbols associated with the codeword in the E-step in (24).

3) Asymptotic EM Algorithm: Combining the results in (30) and (35), in the case of a high SNR and a large dataset size, the asymptotic EM algorithm for detecting the Grassmann codebook $\mathcal{F}$ iterates between the following two steps:

$$\text{(Symbol detection)} \quad \hat{\mathbf{X}}^{(i)} = \arg\min_{\hat{\boldsymbol{\mu}}_\ell \in \hat{\mathcal{F}}} d_p^2 \left(\boldsymbol{\Upsilon}^{(i)}, \hat{\boldsymbol{\mu}}_\ell \right), \quad \forall i, \tag{36}$$

$$\text{(Codeword optimization)} \quad \hat{\boldsymbol{\mu}}_\ell = \arg\min_{\boldsymbol{\mu}_\ell \in \mathcal{G}} \sum_{i \in \mathcal{C}_\ell} d_p^2 (\boldsymbol{\Upsilon}^{(i)}, \boldsymbol{\mu}_\ell), \quad \forall \ell. \tag{37}$$

This is exactly the well-known Grassmann K-means algorithm, thereby relating the ML constellation detection to data clustering on the Grassmannian.

VI. GRASSMANN CONSTELLATION DETECTION BY DATA CLUSTERING

In the preceding section, the ML constellation detection is shown to be asymptotically equivalent to Grassmann data clustering under a high SNR. In this section, building on this connection, several algorithms for Grassmann data clustering are briefly discussed and applied to constellation

---

Algorithm 1 K-means Algorithm for Grassmann Constellation and Symbol Detection

---

Input: A block of Grassmann symbols $\{\mathbf{\Upsilon}^{(i)}\}_{i=1}^{N}$ and the constellation size L.

Output: The estimated codewords $\{\hat{\boldsymbol{\mu}}_\ell\}$ of the Grassmann constellation $\hat{\mathcal{F}}$.

Initialization: Randomly choose L symbols from $\{\mathbf{\Upsilon}^{(i)}\}$ as the initial codewords.

Iterate

- **Step 1 (Symbol Detection)**: Separate the symbols into L clusters each is associated with a single codeword. To this end, assign each Grassmann symbol, say $\mathbf{\Upsilon}^{(i)}$, to the codeword with the shortest geodesic distance, namely $\hat{\mathbf{X}}^{(i)} = \arg \min_{\hat{\boldsymbol{\mu}}_\ell \in \hat{\mathcal{F}}} d_g^2(\mathbf{\Upsilon}^{(i)}, \hat{\boldsymbol{\mu}}_\ell)$.
- **Step 2 (Codeword Optimization)**: For each symbol cluster, update the associated codeword as the sample Karcher mean of the cluster that is computed using Algorithm 2.

Until Convergence

---

detection. Furthermore, it is even possible to detect a Grassmann constellation without the knowledge of the constellation size, which is required by the previously considered EM algorithm for ML detection.

A. Data Clustering with a Known Constellation Size

Consider the case that the constellation size, $L = |\mathcal{F}|$, is known at the receiver. As derived in the preceding section, the Grassmann K-means algorithm for constellation detection iterates between two steps: 1) symbol detection in (36) and 2) codeword optimization in (37) until convergence. An efficient implementation of the algorithm is proposed in [24] and presented in Algorithm 1 that replaces the current Procrustes distance with the geodesic distance as defined in (9). This allows the step of codeword optimization in (37) to be efficiently solved using the following algorithm of *sample Karcher mean*.

Considering a cluster of Grassmann symbols, say $\{i \in \mathcal{C}_\ell\}$, the sample Karcher mean, denoted as $\hat{\boldsymbol{\mu}}_\ell$, can be defined as follows [31]:

$$\hat{\boldsymbol{\mu}}_\ell = \arg \min_{\boldsymbol{\mu}_\ell \in \mathcal{G}} \frac{1}{N_\ell} \sum_{i \in \mathcal{C}_\ell} d_g^2 \left(\boldsymbol{\mu}_\ell, \mathbf{\Upsilon}^{(i)} \right). \tag{38}$$

One can observe that the definition is equivalent to the derived codeword-optimization step in (37) except for replacing the Procrustes distance with the geodesic distance. The algorithm of sample Karcher mean as presented in Algorithm 2 solves the optimization problem in (38) by gradient descend on the Grassmannian [24], [32]. The key idea of the algorithm is computing

---

Algorithm 2 Algorithm of Sample Karcher Mean for Codeword Optimization

---

Input: A block of Grassmann symbols $\{\mathbf{\Upsilon}^{(i)}\}_{i=1}^{M}$.

Output: The Karcher mean of the cluster, denoted as $\boldsymbol{\mu}^*$.

Initialization: Set $\boldsymbol{\mu}^*$ as a randomly selected point from $\{\mathbf{\Upsilon}^{(i)}\}$.

Iterate

- **Step 1**: Project the points in $\{\mathbf{\Upsilon}^{(i)}\}$ onto the tangent space with $\boldsymbol{\mu}_0 = \boldsymbol{\mu}^*$ as the point of tangency by applying the logarithm mapping in (5), i.e., $\mathbf{T}^{(i)} = \log_{\boldsymbol{\mu}_0}(\mathbf{\Upsilon}^{(i)})$.
- **Step 2**: Calculate the mean direction $\bar{\mathbf{T}}$ in the tangent space by averaging: $\bar{\mathbf{T}} = \frac{1}{M} \sum_{i=1}^{M} \mathbf{T}^{(i)}$.
- **Step 3**: Update the Karcher mean $\boldsymbol{\mu}^*$ by moving it in the direction of $\bar{\mathbf{T}}$ via the exponential mapping in (4): $\boldsymbol{\mu}^* = \exp_{\boldsymbol{\mu}_0}(\tau \bar{\mathbf{T}})$, where the step size τ is typically set as 0.5.

Until Convergence.

---

the descend direction on the Grassmannian in a tangent Euclidean space exploiting exponential and logarithm mappings between the two spaces [see (4) and (5)]. Last, it is worth mentioning that besides the Karcher mean, there exist other mean metrics such as *Procrustes mean* and related optimization algorithms [33]. As observed from simulation, the choices of the subspace distance metric (e.g., geodesic versus Procrustes distances) and mean metrics of a cluster of Grassmann symbols (e.g., Karcher versus Procrustes means) seem to have an insignificant effect on the performance of Grassmann constellation detection by data clustering. For this reason, the specific metric in a particular part of analysis is selected for tractability without affecting the resultant general insights.

B. Data Clustering with a Unknown Constellation Size

Consider the case that the constellation size, $L = |\mathcal{F}|$, is unknown at the receiver. Without the knowledge, the K-means algorithm discussed in the last sub-section cannot be applied since it requires L as the input. Specifically, the algorithm relies on randomly choosing L Grassmann symbols as the centroids to generate L clusters. Alternatively, a standard algorithm for *connected-component identification* such as DFS [34] can be applied to recognizing Grassmann symbol clusters by examining the pair-wise subspace distance against a pre-specified threshold denoted as γ_0. The main procedure of the DFS algorithm is summarized in Algorithm 3. Note that a single calling of the DFS algorithm Algorithm outputs only one recognized cluster. As a result, repeatedly implementation of DFS on the remaining unlabelled symbols is needed for resolving

---

Algorithm 3 DFS-Based Algorithm for Grassmann Symbol Clustering

---

Input: The block of Grassmann symbols $\{\mathbf{\Upsilon}^{(i)}\}_{i=1}^{N}$.

Output: All $\{\mathbf{\Upsilon}^{(i)}|\ \mathbf{\Upsilon}^{(i)} \neq \mathbf{\Upsilon}\}$ reachable from $\mathbf{\Upsilon}$ labeled as discovered.

Procedure DFS($\mathcal{M}, \mathbf{\Upsilon}$):

- Label $\mathbf{\Upsilon}$ as discovered.
- **For all** $\{\mathbf{\Upsilon}'\}$ in an adjacent set defined as $\mathcal{A}_{\mathbf{\Upsilon}} = \left\{\mathbf{\Upsilon}^{(i)}|\ d_p\left(\mathbf{\Upsilon}^{(i)}, \mathbf{\Upsilon}\right) \leq \gamma_0\right\}$ **do**
- **If** $\mathbf{\Upsilon}'$ is not labeled as discovered **then** recursively call DFS($\mathcal{M}, \mathbf{\Upsilon}'$).

---

all clusters.

Upon the completion of the DFS algorithm, the constellation size and the estimated codewords can be computed as the number of clusters and their sample Karcher means using (38). Then the received symbols are detected as their associated codewords.

VII. PERFORMANCE OF GRASSMANN CONSTELLATION DETECTION

Due to the difficulty in tractable analysis, there exists few theoretic result on the performance of data clustering while prior work focuses on algorithmic design (see e.g., [24], [34]). In this section, we make an attempt to tackle the challenge by developing a framework for analyzing the performance of data clustering on the Grassmannian in the context of Grassmann constellation detection. In particular, by deriving the conditions of data forming well separable clusters, we can quantify the effects of various system and algorithmic parameters, ranging from the SNR to the connectivity threshold in the DFS algorithm, on the detection performance.

A. Approximate Signal Distribution

A key step in the tractable analysis of Grassmann constellation detection is to approximate the distribution of received signals. Let $\mathsf{span}(\mathbf{A})$ denote a basis spanning the column space of a matrix $\mathbf{A}$. Then it follows from (27) that in the presence of noise, the received Grassmann symbol $\mathbf{\Upsilon}^{(i)}$ is

$$\mathbf{\Upsilon}^{(i)} = \mathsf{span}\left(\mathbf{X}^{(i)} + \sqrt{\frac{N_t}{\rho T}}\mathbf{W}^{(i)}\begin{bmatrix} \lambda_1^{-1} & \cdots & 0 \\ \vdots & \ddots & \vdots \\ 0 & \cdots & \lambda_{N_t}^{-1} \end{bmatrix}\right), \tag{39}$$

where $\mathbf{X}^{(i)}$ is the transmitted (Grassmann) symbol and $\mathbf{W}^{(i)}$ an i.i.d. Gaussian matrix representing noise. The distribution of the random subspace distance of $\mathbf{\Upsilon}^{(i)}$ from the centroid $\mathbf{X}^{(i)}$ determines
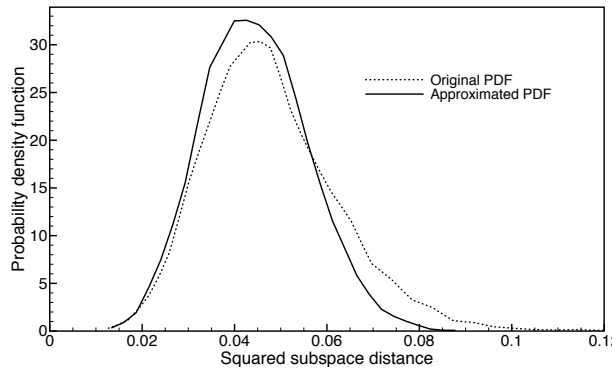
Figure 2. Signal distribution approximation.

the size of received signal cluster centered at $\mathbf{X}^{(i)}$. It is difficult to characterize the distribution due to the eclipse distribution of the noise process after scaling by the inverse channel singular values $\{\lambda_1^{-1}, \cdots, \lambda_{N_t}^{-1}\}$. To overcome the difficulty, replacing all singular values in (39) with the expectation of a typical one, denoted as $\bar{\lambda}$, yields a random orthonormal matrix $\widetilde{\mathbf{\Upsilon}}^{(i)}$ defined as:

$$\widetilde{\mathbf{\Upsilon}}^{(i)} = \mathsf{span}\left(\mathbf{X}^{(i)} + \frac{1}{\bar{\lambda}}\sqrt{\frac{N_t}{\rho T}}\mathbf{W}^{(i)}\right),\tag{40}$$

which results from $\mathbf{X}^{(i)}$ perturbed by isotropic Gaussian noise. Then the distribution of the distance $d_p\left(\mathbf{\Upsilon}^{(i)}, \mathbf{X}^{(i)}\right)$ is approximated by that of $d_p\left(\widetilde{\mathbf{\Upsilon}}^{(i)}, \mathbf{X}^{(i)}\right)$:

$$\text{(Approximate distance distribution)} \quad d_p\left(\mathbf{\Upsilon}^{(i)}, \mathbf{X}^{(i)}\right) \stackrel{\mathrm{d}}{\approx} d_p\left(\widetilde{\mathbf{\Upsilon}}^{(i)}, \mathbf{X}^{(i)}\right),\tag{41}$$

where $\stackrel{\mathrm{d}}{\approx}$ represents approximation in distribution.

Remark 1. (Accurate distance-distribution approximation). The approximation in (41) is accurate in the case that the transmit antennas are far outnumbered by receive ones, i.e., $N_r \gg N_t$, and the resultant large spatial diversity gain makes the channel matrix well conditioned with $\lambda_1 \approx \lambda_2 \cdots \approx \lambda_{N_r}$. Furthermore, empirical results with typical setting $N_t = 2, N_r = 10$ is provided in Fig. 2 to further support the statement.

For convenience, given a codeword $\boldsymbol{\mu}_\ell$, denote $d_p\left(\mathbf{\Upsilon}^{(i)}, \boldsymbol{\mu}_\ell\right)$ and $d_p\left(\widetilde{\mathbf{\Upsilon}}^{(i)}, \boldsymbol{\mu}_\ell\right)$ as $d_\ell^{(i)}$ and $\tilde{d}_\ell^{(i)}$, respectively. Unlike $d_\ell^{(i)}$, the distribution of $\tilde{d}_\ell^{(i)}$ is independent of the direction from $\boldsymbol{\mu}_\ell$ to $\widetilde{\mathbf{\Upsilon}}^{(i)}$ due to the isotropicity of noise in (40). As a result, the distribution of $\tilde{d}_\ell^{(i)}$, which approximates that of the desired r.v. $d_\ell^{(i)}$, can be characterized mathematically. To this end, a useful result is provided.

Lemma 6 ([33]). Let $\mathbf{\Upsilon} = \text{span}(\boldsymbol{\mu} + \mathbf{A})$ with $\boldsymbol{\mu} \in \mathbb{O}^{M \times N}$ and $\mathbf{A}$ an $M \times N$ matrix having i.i.d. $\mathcal{CN}(0, \sigma^2)$ elements. Then given $\boldsymbol{\mu}$ and as $\sigma^2 \to 0$, the distance $d_p(\mathbf{\Upsilon}, \boldsymbol{\mu})$ has the following distribution:

$$[d_p(\mathbf{\Upsilon}, \boldsymbol{\mu})]^2 \sim \sigma^2 \mathcal{X}_D^2, \tag{42}$$

where $D = 2N(M - N)$ and $\mathcal{X}_D^2$ represents a Chi-squared r.v. with D degrees of freedom.

The distance $d_\ell^{(i)}$ defined earlier represents the random deviation of a received symbol from the corresponding transmitted symbol. Using Lemma 6, its distribution is characterized as follows.

Lemma 7. Consider an arbitrary Grassmann codeword $\boldsymbol{\mu}_\ell$ and the approximation in (41). In the high-SNR regime ($\rho \to \infty$), $d_\ell^{(i)} \overset{\text{d}}{\approx} \tilde{d}_\ell^{(i)}$ with the distribution of $\tilde{d}_\ell^{(i)}$ given as

$$\Pr\left(\tilde{d}_\ell^{(i)} \geq r \right) = \frac{1}{\Gamma(\frac{D}{2})} \Gamma\left(\frac{D}{2}, \frac{\rho T \bar{\lambda}^2 r^2}{2N_t} \right), \qquad \forall i \in \mathcal{C}_\ell \tag{43}$$

$$= \frac{\left(\frac{\rho T \bar{\lambda}^2 r^2}{2N_t} \right)^{\frac{D}{2}-1}}{\Gamma(\frac{D}{2})} \exp\left(-\frac{\rho T \bar{\lambda}^2 r^2}{2N_t} \right) \left(1 + o\left(\frac{1}{\rho} \right) \right). \tag{44}$$

with $r \geq 0$ and the upper incomplete Gamma function $\Gamma(D, x) = \int_x^\infty t^{D-1} e^{-t} dt$.

One can observe from the result that $\Pr(d_\ell^{(i)} \geq r)$ decays exponentially as the SNR ρ grows. This suggests that at a high SNR, received symbols tend to cluster around their corresponding transmitted codewords and the clusters shrink rapidly as the SNR grows. This makes them well separated, facilitating constellation detection using a clustering algorithm. This insight is rigorously studied in the following sub-sections building on the approximation in (41) and distance distribution in Lemma 7.

B. Constellation Detection with a Known Size

Considering the case that the receiver has prior knowledge of the constellation size L such that the the K-means algorithm in Algorithm 1 can be applied to constellation detection. For the algorithm to be effective, the received symbols should form well separated clusters on the Grassmannian. In this section, the conditions for forming clusters are derived and then applied to study the effects of system parameters on the algorithmic performance.

First, a metric, called *separability probability*, is defined to measure the level of clustering of the received symbols. To begin with, using the codewords $\{\boldsymbol{\mu}_\ell\}$ in $\mathcal{F}$ as centroids and applying

the nearest-neighbour rule, the Grassmannian $\mathcal{G}_{N_t,T}$ can be partitioned into L *Voronoi cells*. The cell with the centroid $\boldsymbol{\mu}_\ell$ is denoted as $\mathcal{V}(\boldsymbol{\mu}_\ell)$ and defined as

$$\mathcal{V}(\boldsymbol{\mu}_\ell) = \{\boldsymbol{\Upsilon} \in \mathcal{G}_{N_t,T} \mid d_p(\boldsymbol{\Upsilon}, \boldsymbol{\mu}_\ell) < d_p(\boldsymbol{\Upsilon}, \boldsymbol{\mu}_m) \ \forall \ m \neq \ell\}. \tag{45}$$

Intuitively, the received symbol clusters are separable if each of them is contained mostly within the *correct* Voronoi cell, namely the one having the corresponding transmitted codeword as the centroid. Then an effective initiation of the K-mean algorithm (see Algorithm 1), namely the L initial centroids are all within different Voronoi cells, can lead to convergence to their centroids or equivalently the correct detection of the constellation. Inspired by this fact, we define the *separability probability* as the probability that a received Grassmann symbol lies in the correct Voronoi cell. Then a larger separability probability corresponds to a higher level of separability of the received symbol clusters and hence better performance of constellation detection, and vice versa. The mathematical definition of the metric is given below.

Definition 3. (K-means Separability Probability). Let $\mathbf{X}$ denote a typical transmitted symbol and $\boldsymbol{\Upsilon}$ the corresponding received symbol. The *separability probability*, denoted as p_{sep}, is defined as

$$p_{\mathsf{sep}} = \frac{1}{L} \sum_{\ell=1}^{L} \Pr\left(\boldsymbol{\Upsilon} \in \mathcal{V}(\boldsymbol{\mu}_\ell) \mid \mathbf{X} = \boldsymbol{\mu}_\ell\right). \tag{46}$$

Though direct analysis of p_{sep} is difficult, a tractable lower bound can be obtained as follows. For the codebook $\mathcal{F}$, with the minimum codeword pairwise distance $d_{\min}$ defined in (33). The optimal codebook design by packing in (8) attempts to maximize $d_{\min}$. It is well known in the literature of Grassmannian packing that $d_{\min}$ can be bounded as (see e.g., [35])

$$d_{\min}^2 \geq 4N_t \left(\frac{1}{L}\right)^{\frac{1}{TN_t}}. \tag{47}$$

Given $d_{\min}$, a sufficient condition for a cluster of received symbols, say those with the indices $\mathcal{C}_\ell$, originating from the same codeword, say $\boldsymbol{\mu}_\ell$, to be contained within the correct Voronoi cell is:

$$\max_{i \in \mathcal{C}_\ell} d_p(\boldsymbol{\Upsilon}^{(i)}, \boldsymbol{\mu}_\ell) \leq \frac{d_{\min}}{2}.$$

Then jointly considering the sufficient conditions for all clusters of symbols leads to

$$p_{\mathsf{sep}} \geq \Pr\left(\bigcap_{\ell=1}^{L} \max_{i \in \mathcal{C}_\ell} d_p(\boldsymbol{\Upsilon}^{(i)}, \boldsymbol{\mu}_\ell) \leq \frac{d_{\min}}{2}\right). \tag{48}$$

Combining this result and that in Lemma 7 gives the following main result of the sub-section.

Theorem 1 (K-means Separability Probability)**.** Consider Grassmann constellation detection using the K-means algorithm. In the high SNR regime ($\rho \to \infty$), the separability probability satisfies

$$p_{\text{sep}} \geq \left[\frac{1}{\Gamma(\frac{D}{2})} \gamma \left(\frac{D}{2}, \frac{\rho T \bar{\lambda}^2 d_{\min}^2}{8 N_t} \right) \right]^N \tag{49}$$

$$= 1 - N e^{-\frac{\rho T \bar{\lambda}^2 d_{\min}^2}{8 N_t}} G_m(\rho) + O(e^{-2\rho}), \qquad \rho \to \infty, \tag{50}$$

where $G_m(\rho)$ is a polynomial function of ρ defined as $G_m(\rho) = \sum_{m=0}^{\frac{D}{2}-1} \frac{(T \bar{\lambda}^2 d_{\min}^2)^m}{m!(8 N_t)^m} \rho^m$ and γ denotes the lower incomplete Gamma function defined as $\gamma(D, x) = \int_0^x t^{D-1} e^{-t} dt$.

By measuring the performance of constellation detection by the separability probability, the effects of two parameters, the SNR and dataset size, on the performance can be inferred from the result in Theorem 1 as described below.

- **Effect of SNR**: One can observe from (50) that p_{sep} converges to one exponentially fast as ρ grows. Intuitively, in the high SNR regime, the received symbols form highly compact clusters on the Grassmannian. This enhances the pairwise differentiability of the clusters and leads to accurate constellation detection.

- **Effect of Dataset Size**: According to (50), in the high SNR regime, the separability probability may decay linearly with the dataset size N as confirmed by simulation. The reason is that as the dataset size grows, it is more likely that there exist symbols having large distances from the centroids of their correct Voronoi cells. As a result, the separation gaps between clusters narrow or they even overlap, increasing the difficulty in accurate clustering and thereby degrading the detection performance.

- **Dataset-SNR Tradeoff**: Based on (50), the lower bound on p_{sep} can be written in a simple form to reflect the tradeoff between the SNR and dataset size:

$$p_{\text{sep}} \approx 1 - e^{\log N - c\rho}, \qquad \rho \to \infty, \tag{51}$$

with c being a constant. One can infer from the result that under a constraint on the separability probability, as N grows, the SNR should scale up linearly with $\log N$.

- **Effect of Constellation Size**: The dependency of p_{sep} on $d_{\min}^2$ in (50) can be further translated to that on L. Specifically, by substituting (47) to (50),

$$p_{\mathsf{sep}} \approx 1 - a_0 e^{-b_0 \rho L^{-\frac{1}{TN_t}}}, \qquad \rho \to \infty, \tag{52}$$

where a_0 and b_0 are constants. It can be clearly seen that p_{sep} monotonically decreases with respect to L. This aligns with our intuition that packing more constellation points (codewords) on a fixed Grassmann manifold will decrease $d_{\min}$, thus making different clusters harder to be distinguished. Furthermore, one can infer from the result that given a target separability probability, as L grows, the SNR should approximately scale up linearly with $L^{\frac{1}{TN_t}}$.

C. Constellation Detection with an Unknown Size

Considering the case that the constellation size L is unknown at the receiver and the DFS algorithm in Algorithm 3 is applied to constellation detection. The algorithm is based on a different principle from that of the K-means algorithm in the preceding case. While K-means relies on iterative centroid computation and clustering, the DFS attempts to connect neighbouring symbols to form clusters by applying a distance threshold γ_0 (see Algorithm 3), called the DFS threshold. Consequently, two factors of the dataset distribution affect the DFS performance. One is the separability of symbol clusters as for the K-means algorithm, which is measured by the separability probability. By slight abuse of notation, the metric for the DFS is also denoted as p_{sep}. The other is the connectivity within each single cluster, which is unique for the DFS. A metric, called *connectivity probability* and denoted as p_{con}, is defined in the sequel to measure the intra-cluster connectivity of the received dataset. Given the metrics, the effectiveness of constellation detection by the DFS can be ensured by applying constraints on their values:

$$p_{\mathsf{sep}} \geq 1 - \epsilon, \quad p_{\mathsf{con}} \geq 1 - \delta, \tag{53}$$

where $0 < \epsilon, \delta < 1$. In the sequel, p_{sep} and p_{con} are analyzed separately and the results are then combined to quantity the effects the parameters of the system and algorithm on the detection performance.

1) Inter-cluster Separation: For the DFS, the separation between two clusters of Grassmann symbols specified by the index sets $\mathcal{C}_m$ and $\mathcal{C}_\ell$ can be measured by the minimum pairwise

distance, referred to as the *inter-cluster distance* and defined mathematically as

$$d_{\text{clu}}(\mathcal{C}_m, \mathcal{C}_\ell) = \min_{i \in \mathcal{C}_m, j \in \mathcal{C}_\ell} d_p(\boldsymbol{\Upsilon}^{(i)}, \boldsymbol{\Upsilon}^{(j)}). \tag{54}$$

The two clusters can be separated by the DFS when their distance exceeds the DFS threshold γ_0. Based on this fact, the separability probability for the DFS can be defined as follows.

Definition 4. (DFS Separability Probability). For constellation detection using the DSF algorithm, the *separability probability* p_{sep} is defined as

$$p_{\text{sep}} = \Pr\left(\min_{m \neq \ell} d_{\text{clu}}(\mathcal{C}_m, \mathcal{C}_\ell) > \gamma_0\right). \tag{55}$$

Though the direct analysis of p_{sep} is difficult, a lower bound can be derived by designing a sufficient condition for cluster separation. Specifically, given the codebook $\mathcal{F}$ with $d_{\min}$, the symbol clusters are separable in terms of the criterion in (55) if all received symbols deviate from their transmitted codewords no more than a distance of $\frac{d_{\min} - \gamma_0}{2}$ (see Fig. 3). Therefore, p_{sep} can be lower bounded as

$$p_{\text{sep}} \geq \prod_{\ell=1}^{L} \Pr\left(\max_{i \in \mathcal{C}_\ell} d_p(\boldsymbol{\Upsilon}^{(i)}, \boldsymbol{\mu}_\ell) \leq \frac{d_{\min} - \gamma_0}{2}\right). \tag{56}$$

Following the same procedure for deriving Theorem 1, we obtain the following corollary.

Corollary 1 (DFS Separability Probability). Consider Grassmann constellation detection using the DFS algorithm. In the high SNR regime ($\rho \to \infty$), the separability probability satisfies

$$p_{\text{sep}}(\rho, L, N, \gamma_0) \geq \left[\frac{1}{\Gamma(\frac{D}{2})} \gamma\left(\frac{D}{2}, \frac{\rho T \bar{\lambda}^2 (d_{\min} - \gamma_0)^2}{8N_t}\right)\right]^N \tag{57}$$

$$= 1 - N e^{-\frac{\rho T \bar{\lambda}^2 (d_{\min} - \gamma_0)^2}{8N_t}} C_m(\rho) + O(e^{-2\rho}), \tag{58}$$

where $C_m(\rho)$ is a polynomial function of ρ defined as $C_m(\rho) = \sum_{m=0}^{\frac{D}{2}-1} \frac{(T\bar{\lambda}^2(d_{\min}-\gamma_0)^2)^m}{m!(8N_t)^m} \rho^m$.

The effects of the parameters including SNR, dataset size and constellation size are similar to their K-means counterparts discussed in the preceding sub-section. A remark is given below on the effect of the DFS threshold γ_0.

Remark 2 (Effect of DFS Threshold). Choosing a too small value of the threshold γ_0 leads to the failure of connecting points within a same cluster and thereby causes it to be split into multiple clusters. On the other hand, if γ_0 is too large, multiple clusters may be connected into
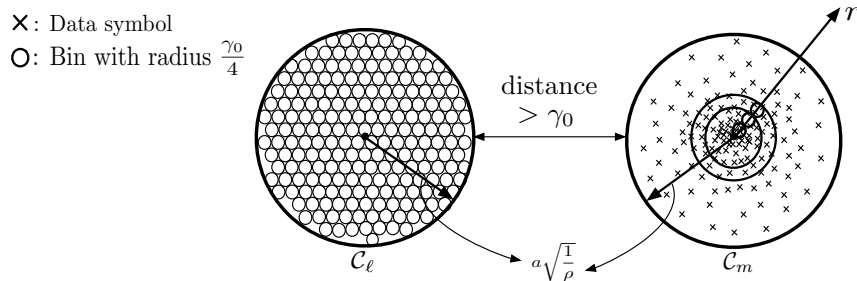
Figure 3. Illustration of pairwise clusters.

a single one. Both cases lead to incorrect constellation detection. Thus γ_0 should be optimized in practice to balance inter-cluster separability and intra-cluster connectivity.

2) Intra-cluster Connectivity: The analysis of intra-cluster connectivity is much more challenging than that of inter-cluster separation. In the context of DFS, two points on the Grassmannian are *neighbours* if their subspace distance is shorter than γ_0. A path is a sequence of points where every pair of adjacent points are neighbours. Then two points are *connected* if there exists a path connecting them. Based on this definition, the direct analysis of connectivity probability is intractable. Inspired by the analysis in the classic area of network connectivity (see e.g, [36]), we develop a geometric technique for deriving a lower bound on the metric and its principle is described as follows.

Principle of Connectivity Analysis: Consider a cluster of points (symbols) on the Grassmannian that are bounded by a disk. The disk is then packed by uniform bins (small disks) each with a diameter $\frac{\gamma_0}{2}$ as illustrated in Fig. 3. As a result, a sufficient condition for all points in the cluster being connected is that all bins are non-empty, namely that each bin contains at least one point. The probability of this event can be derived in closed form that lower bounds the connectivity probability.

Based on the principle, the specific mathematical technique is developed and the desired result obtained as follows. First, for ease of exposition, consider the (intra-cluster) *disconnect probability* defined as $p_{\text{dis}} = 1 - p_{\text{con}}$. Consider the symbols cluster corresponding to the transmitted codeword $\boldsymbol{\mu}_\ell$. Let $p_{\text{dis}}(N_\ell)$ denote the disconnect probability for the cluster conditioned the cluster size N_ℓ. Then $p_{\text{dis}} = \mathbb{E}[p_{\text{dis}}(N_\ell)]$. Since the L codewords have equal probabilities to be transmitted, N_ℓ follows the binomial distribution with parameters N and $1/L$, i.e. $N_\ell \sim B\left(N, \frac{1}{L}\right)$.

Next, consider a cluster of symbols originating from the same transmitted codeword $\boldsymbol{\mu}$. A

disk with the centroid $\boldsymbol{\mu}$ and a radius r is defined on the Grassmannian as $\mathcal{B}(\boldsymbol{\mu}, r) = \{\boldsymbol{\Phi} \in \mathcal{G} \mid d_p(\boldsymbol{\Phi}, \boldsymbol{\mu}) \leq r\}$. It is known in the literature that in the presence of Gaussian noise, the received symbols with the transmitted codeword $\boldsymbol{\mu}$ lie with high probability in a disk $\mathcal{B}(\boldsymbol{\mu}, r)$, whose radius r is proportional to the standard deviation of noise or equivalently proportional to $\frac{1}{\sqrt{\rho}}$ with ρ being the SNR [11], [14]. Therefore, the disk radius can be chosen as $\frac{a}{\sqrt{\rho}}$ with a being a constant (see Fig. 3). The constant can be appropriately chosen such that a symbol lies within the disk with probability no smaller than e.g., $(1 - \frac{\epsilon}{N})$, which, as implied by (58), is sufficient for satisfying the separability constraint in (53).

Assumption 2. The dataset size N is sufficiently large such that the points within each disk are dense. Then the required DFS threshold γ_0 for connecting the points within a disk is much smaller than its radius: $\gamma_0 \ll \frac{a}{\sqrt{\rho}}$.

Based on the assumption, the disk can be packed with small disks each with the diameter $\frac{\gamma_0}{2}$, called *bins*, as illustrated in Fig. 3. Each of the bins thus is placed contacted with at least one another bin. The cluster of symbols can be treated as i.i.d. random points. A bin is nonempty if it contains at least one point. In the event that all bins are nonempty, all points are guaranteed to be connected regardless of if they are inside or outside bins. Therefore, given that the number of points in the cluster is N_ℓ, the corresponding disconnect probability can be lower bounded as

$$p_{\mathsf{dis}}(N_\ell) \leq \Pr(\exists \text{ one empty bin} | N_\ell). \tag{59}$$

Note that the number of bins in the disk is $M = \eta_D \left(\frac{\frac{a}{\sqrt{\rho}}}{\frac{\gamma_0}{4}} \right)^D$ where η_D represents the fraction of the disk area covered by bins which is a constant given the space dimensions of D. Define an indicator function $\mathbb{I}(\mathcal{A}_i) = 1$ if the ith bin is empty, and $\mathbb{I}(\mathcal{A}_i) = 0$ otherwise. The inequality in (59) can be rewritten by

$$p_{\mathsf{dis}}(N_\ell) \leq \Pr \left(\sum_{i=1}^M \mathbb{I}(\mathcal{A}_i) \geq 1 | N_\ell \right), \tag{60}$$

By applying Markov inequality,

$$p_{\mathsf{dis}}(N_\ell) \leq \mathbb{E} \left(\sum_{i=1}^M \mathbb{I}(\mathcal{A}_i) | N_\ell \right) = \sum_{i=1}^M (1 - p_i)^{N_\ell}, \tag{61}$$

where p_i denotes the probability that a typical point falls into the ith bin. Define $p_{\min} = \min_i p_i$.

It follows from (60) that

$$p_{\text{dis}}(N_\ell) \leq M(1 - p_{\min})^{N_\ell}. \tag{62}$$

By invoking the Binomial distribution of N_ℓ,

$$p_{\text{dis}} = \mathbb{E}[p_{\text{dis}}(N_\ell)] \leq M \left(1 - \frac{p_{\min}}{L} \right)^N.$$

Then the result below follows.

Lemma 8. In the high SNR regime, the disconnect probability satisfies: $p_{\text{dis}} \leq M e^{-\frac{p_{\min}}{L} N}$.

Next, to obtain a concrete upper bound on p_{dis}, an expression is derived for $p_{\min}$ as follows. In the presence of isotropic noise, the probability that a receive symbol $\mathbf{\Upsilon}$ originating from a codeword $\boldsymbol{\mu}$ falls into a bin $\mathcal{B}(\mathbf{\Phi}, \frac{\gamma_0}{4})$ depends on the distance $d_p(\mathbf{\Phi}, \boldsymbol{\mu})$ as well as the bin volume, denoted as Vol_{bin}, but is independent of the direction from $\boldsymbol{\mu}$ to $\mathbf{\Phi}$. Define a ring with the center $\boldsymbol{\mu}$, width $\frac{\gamma_0}{2}$, and radius r as $\mathcal{R}(\boldsymbol{\mu}, r) = \{\mathbf{\Phi} \in \mathcal{G} \mid r - \frac{\gamma_0}{2} \leq d_p(\mathbf{\Phi}, \boldsymbol{\mu}) \leq r\}$ which is illustrated in Fig. 3. Then the symbol $\mathbf{\Upsilon}$ falls with equal probabilities into the bins lying in a same ring $\mathcal{R}(\boldsymbol{\mu}, r)$. Let the probability be denoted as $p(r)$ and the volume of the ring as $\text{Vol}_{\text{rin}}(r)$. Then

$$p(r) = \frac{\eta_D^{-1} \text{Vol}_{\text{bin}}(r)}{\text{Vol}_{\text{rin}}(r)} \times \Pr \left(r - \frac{\gamma_0}{2} \leq d_p(\mathbf{\Upsilon}, \boldsymbol{\mu}) \leq r \right)$$

$$\overset{(a)}{=} \frac{\eta_D^{-1} (\frac{\gamma_0}{4})^D}{r^D - (r - \frac{\gamma_0}{2})^D} \times \frac{1}{\Gamma(\frac{D}{2})} \left\{ \Gamma \left(\frac{D}{2}, \frac{\rho T \bar{\lambda}^2 (r - \frac{\gamma_0}{2})^2}{2 N_t} \right) - \Gamma \left(\frac{D}{2}, \frac{\rho T \bar{\lambda}^2 r^2}{2 N_t} \right) \right\}, \quad (r \geq \frac{\gamma_0}{2}), \tag{63}$$

where $D = 2N_t(T - N_t)$ is the dimensions and (a) applies the distance distribution in (42). Given $p(r)$, $p_{\min}$ can be equivalently written as $p_{\min} = \min_{\frac{\gamma_0}{2} \leq r \leq \frac{a}{\sqrt{\rho}}} p(r)$. By analyzing the derivative of $p(r)$, it is straightforward to prove that the function is monotonically decreasing in the range of $r \geq \frac{\gamma_0}{2}$ (see Appendix D), leading to the following result.

Lemma 9. If the disk radius $\frac{a}{\sqrt{\rho}} \geq \frac{\gamma_0}{2}$, $p_{\min} = p \left(\frac{a}{\sqrt{\rho}} \right)$ with $p(r)$ given in (63).

The above lemma shows that the bin with $p_{\min}$ locates at the boundary of the disk. Under Assumption 2 and using (63) and Lemma 9, a simplified asymptotic expression for $p_{\min}$ can be derived as:

$$p_{\min} = \frac{\eta_D^{-1} 2^{-\frac{5D}{2}+1}}{D \Gamma \left(\frac{D}{2} \right)} \left(\frac{T \bar{\lambda}^2}{N_t} \right)^{\frac{D}{2}} \gamma_0^D \rho^{\frac{D}{2}} e^{-\frac{a^2 T \bar{\lambda}^2}{2 N_t}} + o(\gamma_0^D \rho^{\frac{D}{2}}). \tag{64}$$

The derivation details can be found in Appendix E. Finally, substituting (64) and $M = \eta_D \left(\frac{4a}{\gamma_0 \sqrt{\rho}} \right)^D$ into the result in Lemma 8, we can derive a lower bound of the success probability of intra-cluster connectivity, which is presented as follows.

Theorem 2 (DFS Connectivity Probability)**.** In the high SNR regime, the connectivity probability satisfies

$$p_{\mathsf{con}} \geq 1 - \eta_D (4a)^D \gamma_0^{-D} \rho^{-\frac{D}{2}} e^{-c_0 \gamma_0^D \rho^{\frac{D}{2}} \frac{N}{L}}, \tag{65}$$

where $c_0 = \frac{\eta_D^{-1} 2^{-\frac{5D}{2}+1}}{D\Gamma\left(\frac{D}{2}\right)} \left(\frac{T\bar{\lambda}^2}{N_t} \right)^{\frac{D}{2}} e^{-\frac{a^2 T \bar{\lambda}^2}{2N_t}}$ is a constant and N/L denotes the expected number of received symbols in each cluster.

3) Effects of Parameters on Detection Performance: Comparing the results in Corollary 1 and Theorem 2, we obtain the following insights into the effects on various parameters on the constellation detection performance.

- **Effect of SNR**: One can observe from (58) and (65) that both p_{sep} and p_{con} converge *exponentially* to one as ρ grows. A higher SNR makes the dataset distributed in more concentrated clusters centered at the codewords, improving their separability and connectivity in terms of p_{sep} and p_{con}, respectively.

- **Effect of Dataset Size**: Unlike the SNR, the effect of increasing N is double-sided. On one hand, (65) suggests that the intra-cluster connectivity improves exponentially with growing N due to the increasing point-density of each cluster. On the other hand, (58) shows that the separability between clusters may decrease exponentially as N increases. This is because that increasing N may shorten the *inter-cluster distance* defined in (54) due to the more likely existence of "outliers" and the resultant growth of cluster radius.

- **Effect of Constellation Size**: Last, a larger constellation size L reduces both p_{sep} and p_{con} and makes it harder to perform accurate detection by DFS algorithm. Specifically, one can observe from (57) that the separability of different clusters reduces as L increases. This is aligned with our intuition that packing more constellations points on a fixed Grassmann manifold reduces $d_{\min}$, thereby increasing the difficulty of clustering in the presence of noise. Moreover, given the dataset size N, as suggested by (65), a smaller L benefits intra-cluster connectivity since each cluster is expected to comprise more points (the expected number of points is given by N/L), thus denser clusters are formed.

Bits	Mapping	Codewords	$d_p(\mathbf{F}, \boldsymbol{\mu}_\ell^*)$
			descending
11	←——→	$\boldsymbol{\mu}_1^*$	
10	←——→	$\boldsymbol{\mu}_2^*$	
01	←——→	$\boldsymbol{\mu}_3^*$	
00	←——→	$\boldsymbol{\mu}_4^*$	

Figure 4. Illustration of bit-symbol-mapping for constellation size of four.

VIII. Constellation Embedded Bit-Symbol Mapping

Given the inferred constellation codewords, the information retrieval process contains two substeps: 1) associate the observed data to the closest constellation codeword in terms of their distance; 2) map the codeword to corresponding bit sequence according to a pre-defined mapping rule. In this sub-section, we aim to propose an intelligent mechanism for resolving the mapping between the constellation codewords and the embedded information bits without compromising the spectrum efficiency. Specifically, the novel scheme we proposed encodes the mapping information to the subspace distance between the transmit codewords and a well-devised orthonormal reference point such as a truncated Fourier matrix, denoted by $\mathbf{F}$. Concretely, the transmit codewords are one-to-one mapped to a set of information bits following a pre-defined order determined by their subspace distances to the selected reference point (see Fig. 4). The order that encodes the mapping information can be accurately recovered at the receiver since the subspace distances between codewords and $\mathbf{F}$ are invariant to the channel rotation. Note that the reference point should be carefully selected to ensure the subspace distance differentiation to each codeword. To this end, two candidate schemes are proposed: 1) fix a reference point first and select from a set of packing based codebooks the one having the most differentiation of subspace distances; 2) fix a packing based codebook first and then choose the optimal in terms of subspace distance differentiation. The advantage of the scheme 2) over 1) is that codewords only need to be generated once, but at the additional expense of reference point transmission. Note that communicating the reference point can incur overhead (coding and high power) due to the requirement of high accuracy as it affects the detection of all data. The tradeoff between the decoding accuracy and the communication overhead is non-trivial but out of the scope of the paper and leaves for future work.
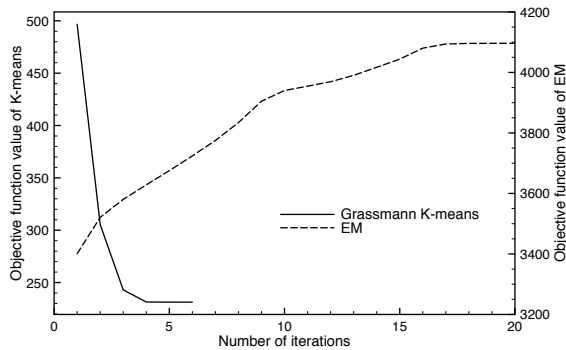
Figure 5.   Convergence-rate comparison between K-means and EM algorithms for Grassmann constellation detection.

IX. SIMULATION RESULTS

The default simulation settings are as follows. The numbers of antennas are $N_r = 4, N_t = 2$. The channel follows block fading channel model and channel coefficients i.i.d. $\mathcal{CN}(0,1)$ r.v.. The noise follows the same distribution. The constellation size and symbol length are $L = 8$ and $T = 4$.

Consider the equivalence of Grassmann K-means and EM algorithms derived in Section V. Their convergence rates are compared in Fig. 5. One can observe that the former converges faster than the latter. This aligns with the discussion in Section V-A2 and confirms the advantage of the proposed data-clustering approach for Grassmann constellation detection.

In Fig. 6, we compare the performance of Grassmann constellation detection with and without the prior knowledge of constellation size L, which are implemented using the K-means and DFS algorithms respectively. Furthermore, each of key parameters is varied to demonstrate its effect on the detection performance and thereby corroborate the analytical results. Define the *successful detection probability* as the probability that the received symbols are correctly clustered according to their corresponding transmitted codewords. Using this metric for measuring the detection performance and by observing Fig. 6(a)-(c), the K-means is observed to substantially outperform the DFS, showing the value of the prior knowledge. Next, comparing Fig. 6(a) and 6(b) reveals that the detection performance can be monotonically improved by increasing the SNR or reducing the constellation size L, which agrees with the insights from the analysis. On the other hand, as observed from Fig. 6(c), increasing the dataset size N can have opposite effects on DFS performance but continuously degrades the K-means performance. The reason is revealed in the analysis: large N improves the intra-cluster connectivity of DFS but degrades its inter-cluster separability while K-means performance only concerns separability. In particular, the

(a) Effect of SNR

(b) Effect of constellation size

(c) Effect of dataset size

(d) Effect of DFS threshold
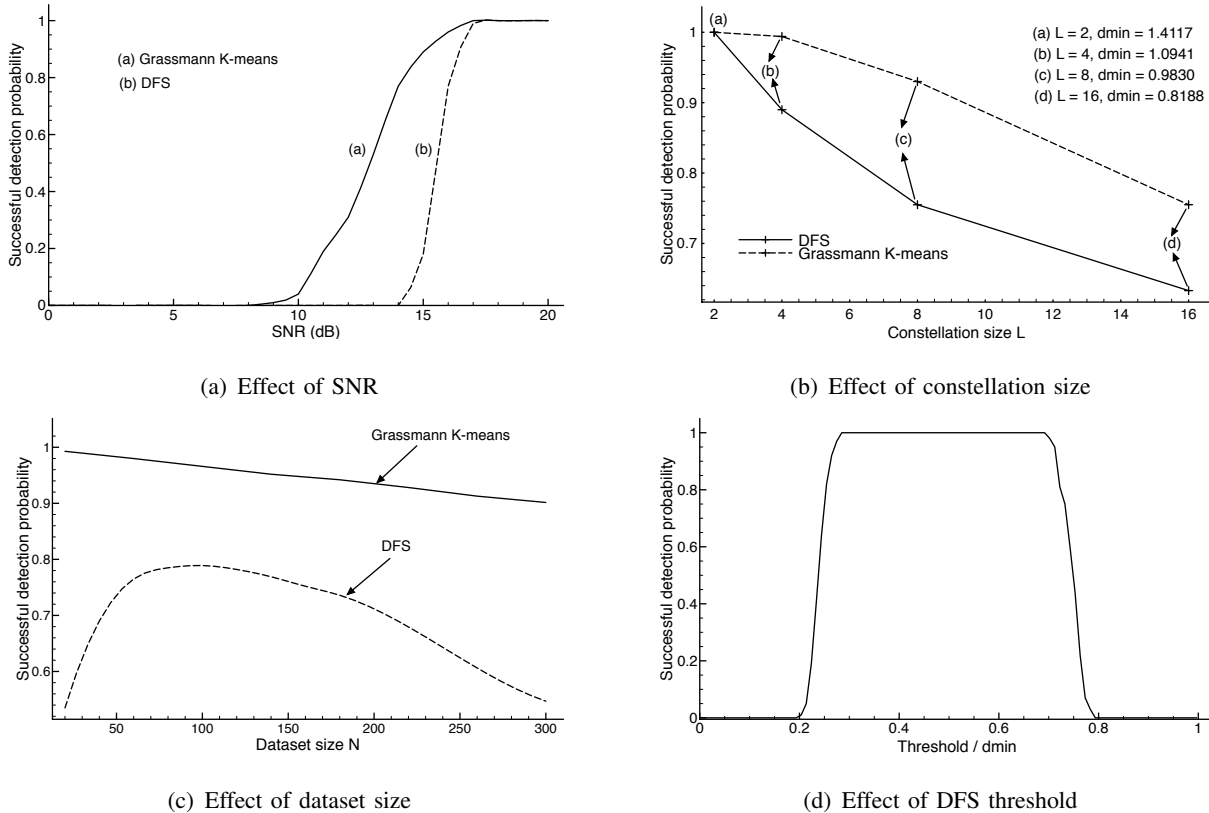
Figure 6. Comparison of Grassmann constellation detection with and without knowledge of constellation size and the effects of parameters.

linear decay rate of success detection probability for K-means is predicted in (50). Last, Fig. 6(d) shows the sensitivity of the DFS performance towards the changes on the DFS threshold and thus its optimization is important, which agrees with the analysis in Section VII-C.

X. CONCLUDING REMARKS

We have proposed an approach of automatic recognition of Grassmann constellations and developed an analytical framework for performance analysis. The work makes contributions to next-generation intelligent radios and opens up several interesting directions for further research including multiuser constellation detection and detection using more complex machine learning tools such as deep learning.

APPENDIX

A. Proof of Lemma 3

According to (27), one can decompose the eigenspace of the received signal as:

$$\mathbf{Y}^{(i)} = \mathbf{U}_Y^{(i)} \mathbf{\Sigma}_Y^{(i)} (\mathbf{V}_Y^{(i)})^H + \mathbf{U}_W^{(i)} \mathbf{\Sigma}_W^{(i)} (\mathbf{V}_W^{(i)})^H. \tag{66}$$

where the first term captures the dominant signal subspace while the second one corresponds to the noise subspace. In the high SNR regime, the noise is negligible and we have the following result

$$\mathbf{Y}^{(i)} = \mathbf{U}_Y^{(i)} \mathbf{\Sigma}_Y^{(i)} (\mathbf{V}_Y^{(i)})^H, \qquad \rho \to \infty. \tag{67}$$

It follows that

$$\mathrm{tr}\left\{ (\mathbf{Y}^{(i)})^H \hat{\boldsymbol{\mu}}_j \hat{\boldsymbol{\mu}}_j^H \mathbf{Y}^{(i)} \right\} \longrightarrow \mathrm{tr}\left\{ (\mathbf{\Sigma}_Y^{(i)})^2 (\mathbf{U}_Y^{(i)})^H \hat{\boldsymbol{\mu}}_j \hat{\boldsymbol{\mu}}_j^H \mathbf{U}_Y^{(i)} \right\}, \qquad \rho \to \infty. \tag{68}$$

With $\mathbf{b}_k$ denoting the kth column of the matrix $\hat{\boldsymbol{\mu}}_j^H \mathbf{U}_Y^{(i)}$ and $\left\{ \sigma_k^{(i)} \right\}_{k=1}^{N_t}$ singular values of $\mathbf{\Sigma}_Y^{(i)}$,

$$\mathrm{tr}\left\{ (\mathbf{\Sigma}_Y^{(i)})^2 (\mathbf{U}_Y^{(i)})^H \hat{\boldsymbol{\mu}}_j \hat{\boldsymbol{\mu}}_j^H \mathbf{U}_Y^{(i)} \right\} = \sum_{k=1}^{N_t} \left(\sigma_k^{(i)} \right)^2 \|\mathbf{b}_k\|^2. \tag{69}$$

By replacing $\left\{ \sigma_k^{(i)} \right\}$ with the largest singular value denoted as $\sigma_1^{(i)}$,

$$\mathrm{tr}\left\{ (\mathbf{Y}^{(i)})^H \hat{\boldsymbol{\mu}}_j \hat{\boldsymbol{\mu}}_j^H \mathbf{Y}^{(i)} \right\} \leq \left(\sigma_1^{(i)} \right)^2 \mathrm{tr}\left\{ (\mathbf{U}_Y^{(i)})^H \hat{\boldsymbol{\mu}}_j \hat{\boldsymbol{\mu}}_j^H \mathbf{U}_Y^{(i)} \right\}, \qquad \rho \to \infty. \tag{70}$$

Similarly, the lower bound of $\mathrm{tr}\left\{ (\mathbf{Y}^{(i)})^H \hat{\boldsymbol{\mu}}_j \hat{\boldsymbol{\mu}}_j^H \mathbf{Y}^{(i)} \right\}$ can be obtained by replacing $\left\{ \sigma_k^{(i)} \right\}$ in (69) with the smallest singular value denoted as $\sigma_{N_t}^{(i)}$:

$$\mathrm{tr}\left\{ (\mathbf{Y}^{(i)})^H \hat{\boldsymbol{\mu}}_j \hat{\boldsymbol{\mu}}_j^H \mathbf{Y}^{(i)} \right\} \geq \left(\sigma_{N_t}^{(i)} \right)^2 \mathrm{tr}\left\{ (\mathbf{U}_Y^{(i)})^H \hat{\boldsymbol{\mu}}_j \hat{\boldsymbol{\mu}}_j^H \mathbf{U}_Y^{(i)} \right\}, \qquad \rho \to \infty. \tag{71}$$

Given that $\mathbf{U}_Y^{(i)} = \mathbf{\Upsilon}^{(i)}$,

$$\left(\sigma_{N_t}^{(i)} \right)^2 \mathrm{tr}\left\{ (\mathbf{\Upsilon}^{(i)})^H \hat{\boldsymbol{\mu}}_j \hat{\boldsymbol{\mu}}_j^H \mathbf{\Upsilon}^{(i)} \right\} \leq \mathrm{tr}\left\{ (\mathbf{Y}^{(i)})^H \hat{\boldsymbol{\mu}}_j \hat{\boldsymbol{\mu}}_j^H \mathbf{Y}^{(i)} \right\} \leq \left(\sigma_1^{(i)} \right)^2 \mathrm{tr}\left\{ (\mathbf{\Upsilon}^{(i)})^H \hat{\boldsymbol{\mu}}_j \hat{\boldsymbol{\mu}}_j^H \mathbf{\Upsilon}^{(i)} \right\}. \tag{72}$$

Rewriting the bounds in (72) in terms of Procrustes distance defined in (10) gives the desired result.

B. Proof of Lemma 4

Let p_ℓ denote the joint probability of two events, namely $\mathcal{A}$: a symbol generated from the ℓ-th codeword and $\mathcal{B}$: a symbol is assigned to cluster ℓ. One can easily see that $N_\ell \geq p_\ell N$. Therefore, as long as p_ℓ is bounded by some strictly positive value, the statement holds. To show this, according to the equal-probability codeword assumption, we have $p(\mathcal{A}) = \frac{1}{L}$, and by definition we also have $p(\mathcal{B}|\mathcal{A}) \geq p(d_p(\boldsymbol{\Upsilon}, \boldsymbol{\mu}) \leq \frac{d_{\min}}{2})$. It follows that $p_\ell \geq \frac{1}{L} p(d_p(\boldsymbol{\Upsilon}, \boldsymbol{\mu}) \leq \frac{d_{\min}}{2})$, where $p(d_p(\boldsymbol{\Upsilon}, \boldsymbol{\mu}) \leq \frac{d_{\min}}{2})$ can be directly derived from Lemma 7. Thus p_ℓ is indeed strictly positive. Consequently, $N \to \infty$ can lead to $N_\ell \to \infty$, completing the proof.

C. Proof of Lemma 5

By substituting $\boldsymbol{\mu}_\ell^* \mathbf{H}^{(i)} + \sqrt{\frac{N_t}{\rho T}} \mathbf{W}^{(i)}$ into $\mathbf{Y}^{(i)}$, $\frac{1}{N_\ell} \sum_{i \in \mathcal{C}_\ell} \mathrm{tr}\left\{ (\mathbf{Y}^{(i)})^H \boldsymbol{\mu}_\ell \boldsymbol{\mu}_\ell^H \mathbf{Y}^{(i)} \right\}$ can be rewritten as

$$\frac{1}{N_\ell} \sum_{i \in \mathcal{C}_\ell} \mathrm{tr}\left\{ \left(\boldsymbol{\mu}_\ell^* \mathbf{H}^{(i)} + \sqrt{\frac{N_t}{\rho T}} \mathbf{W}^{(i)} \right) \left(\boldsymbol{\mu}_\ell^* \mathbf{H}^{(i)} + \sqrt{\frac{N_t}{\rho T}} \mathbf{W}^{(i)} \right)^H \boldsymbol{\mu}_\ell \boldsymbol{\mu}_\ell^H \right\}. \tag{73}$$

Using the law of large numbers, as $N_\ell \to \infty$, $\frac{1}{N_\ell} \sum_{i \in \mathcal{C}_\ell} \mathrm{tr}\left\{ (\mathbf{Y}^{(i)})^H \boldsymbol{\mu}_\ell \boldsymbol{\mu}_\ell^H \mathbf{Y}^{(i)} \right\}$ can thus be simplified as

$$\frac{1}{N_\ell} \sum_{i \in \mathcal{C}_\ell} \mathrm{tr}\left\{ (\mathbf{Y}^{(i)})^H \boldsymbol{\mu}_\ell \boldsymbol{\mu}_\ell^H \mathbf{Y}^{(i)} \right\} \longrightarrow \mathrm{tr}\left\{ \boldsymbol{\mu}_\ell^* (\boldsymbol{\mu}_\ell^*)^H \boldsymbol{\mu}_\ell \boldsymbol{\mu}_\ell^H \right\} + \frac{N_t^2}{\rho T}. \tag{74}$$

Let $\mathbf{Q}^{(i)}$ denote the unitary matrix,

$$\mathrm{tr}\left\{ \boldsymbol{\mu}_\ell^* (\boldsymbol{\mu}_\ell^*)^H \boldsymbol{\mu}_\ell \boldsymbol{\mu}_\ell^H \right\} = \mathrm{tr}\left\{ \frac{1}{N_\ell} \left(\sum_{i \in \mathcal{C}_\ell} (\boldsymbol{\mu}_\ell^* \mathbf{Q}^{(i)})(\boldsymbol{\mu}_\ell^* \mathbf{Q}^{(i)})^H \right) \boldsymbol{\mu}_\ell \boldsymbol{\mu}_\ell^H \right\}. \tag{75}$$

Moreover, as $\rho \to \infty$, the noise effect is negligible, resulting in $\mathbf{U}_Y^{(i)} \to \boldsymbol{\mu}_\ell^* \mathbf{Q}^{(i)} = \boldsymbol{\Upsilon}^{(i)}$. This can be interpreted as as an approximation of the column space spanned by the received signal $\mathbf{Y}^{(i)}$. Thereby, we have the following result.

$$\frac{1}{N_\ell} \sum_{i \in \mathcal{C}_\ell} \mathrm{tr}\left\{ (\mathbf{Y}^{(i)})^H \boldsymbol{\mu}_\ell \boldsymbol{\mu}_\ell^H \mathbf{Y}^{(i)} \right\} \longrightarrow \frac{1}{N_\ell} \sum_{i \in \mathcal{C}_\ell} \mathrm{tr}\left\{ \boldsymbol{\Upsilon}^{(i)} (\boldsymbol{\Upsilon}^{(i)})^H \boldsymbol{\mu}_\ell \boldsymbol{\mu}_\ell^H \right\}, \qquad \rho \to \infty. \tag{76}$$

This completes the proof.

D. Proof of monotonous decreasing property of $p(r)$

Note that the first term in (63), i.e. $\frac{\eta_D^{-1} (\frac{\gamma_0}{4})^D}{r^D - (r - \frac{\gamma_0}{2})^D}$, decreases monotonically with respect to r, hence, it is sufficient to prove the monotonically decreasing characteristics of the second term

for $r \geq \frac{\gamma_0}{2}$. By defining $f(r) = \Gamma\left(\frac{D}{2}, \frac{\rho T \bar{\lambda}^2 (r - \frac{\gamma_0}{2})^2}{2N_t}\right) - \Gamma\left(\frac{D}{2}, \frac{\rho T \bar{\lambda}^2 r^2}{2N_t}\right)$ and setting its first derivative to 0, the following equality holds

$$\frac{\gamma_0}{2r} = 1 - e^{-\frac{\rho T \bar{\lambda}^2 \gamma_0 (r - \frac{\gamma_0}{4})}{2N_t (D-1)}}. \tag{77}$$

Observe that as $\rho \to \infty$, $e^{-\frac{\rho T \bar{\lambda}^2 \gamma_0 (r - \frac{\gamma_0}{4})}{2N_t (D-1)}} \to 0$, we thus have $r = \frac{\gamma_0}{2}$, which implies that $f(r)$ decreases monotonically for $r \geq \frac{\gamma_0}{2}$. We complete the whole proof.

E. Computation of $p_{\min}$

By substituting x in (63) with $\frac{a}{\sqrt{\rho}}$, we have

$$p_{\min} = \frac{\eta_D^{-1} (\frac{\gamma_0}{4})^D}{\Gamma(\frac{D}{2}) \left((\frac{a}{\sqrt{\rho}})^D - (\frac{a}{\sqrt{\rho}} - \frac{\gamma_0}{2})^D \right)} \left\{ \Gamma\left(\frac{D}{2}, \frac{\rho T \bar{\lambda}^2 \left(\frac{a}{\sqrt{\rho}} - \frac{\gamma_0}{2} \right)^2}{2N_t} \right) - \Gamma\left(\frac{D}{2}, \frac{T \bar{\lambda}^2 a^2}{2N_t} \right) \right\}. \tag{78}$$

Next, consider $\Gamma\left(\frac{D}{2}, \frac{\rho T \bar{\lambda}^2 \left(\frac{a}{\sqrt{\rho}} - \frac{\gamma_0}{2} \right)^2}{2N_t} \right) = \Gamma\left(\frac{D}{2}, \frac{a^2 T \bar{\lambda}^2 + \rho T \bar{\lambda}^2 \frac{\gamma_0^2}{4} - a \gamma_0 T \bar{\lambda}^2 \sqrt{\rho}}{2N_t} \right)$. Under the assumption that $\frac{\gamma_0}{2} \ll \frac{a}{\sqrt{\rho}}$, we have $\frac{\rho T \bar{\lambda}^2 \frac{\gamma_0^2}{4}}{a \gamma_0 T \bar{\lambda}^2 \sqrt{\rho}} = \frac{1}{2} \frac{\frac{\gamma_0}{2}}{\frac{a}{\sqrt{\rho}}} \to 0$, holds. Ignoring the high-order term $\rho T \bar{\lambda}^2 \frac{\gamma_0^2}{4}$, one can have

$$\Gamma\left(\frac{D}{2}, \frac{\rho T \bar{\lambda}^2 \left(\frac{a}{\sqrt{\rho}} - \frac{\gamma_0}{2} \right)^2}{2N_t} \right) = \Gamma\left(\frac{D}{2}, \frac{a^2 T \bar{\lambda}^2 - a \gamma_0 T \bar{\lambda}^2 \sqrt{\rho}}{2N_t} \right) + o(\gamma_0^D \rho^{\frac{D}{2}})$$

$$= \Gamma\left(\frac{D}{2}, \frac{a^2 T \bar{\lambda}^2}{2N_t} \right) + \int_{\frac{a^2 T \bar{\lambda}^2 - a \gamma_0 T \bar{\lambda}^2 \sqrt{\rho}}{2N_t}}^{\frac{a^2 T \bar{\lambda}^2}{2N_t}} x^{\frac{D}{2}-1} e^{-x} dx + o(\gamma_0^D \rho^{\frac{D}{2}}). \tag{79}$$

Realizing the fact that $\frac{a \gamma_0 T \bar{\lambda}^2 \sqrt{\rho}}{a^2 T \bar{\lambda}^2} = \frac{\gamma_0}{\frac{a}{\sqrt{\rho}}} \to 0$, the second term of (79) can be rewritten as

$$\int_{\frac{a^2 T \bar{\lambda}^2 - a \gamma_0 T \bar{\lambda}^2 \sqrt{\rho}}{2N_t}}^{\frac{a^2 T \bar{\lambda}^2}{2N_t}} x^{\frac{D}{2}-1} e^{-x} dx = x_0^{\frac{D}{2}-1} e^{-x_0} \Delta x_0 + o(\gamma_0 \sqrt{\rho}), \tag{80}$$

where $\Delta x_0 = \frac{a \gamma_0 T \bar{\lambda}^2 \sqrt{\rho}}{2N_t}$, $x_0 = \frac{a^2 T \bar{\lambda}^2}{2N_t}$. Moreover, since $x^D - \left(x - \frac{\gamma_0}{2} \right)^D = \frac{D \gamma_0}{2} x^{D-1} + o(\gamma_0 x^{D-1})$ for $\frac{\gamma_0}{2} \ll x$, which can be directly proved using *Taylor expansion*, we thus have

$$\left(\frac{a}{\sqrt{\rho}} \right)^D - \left(\frac{a}{\sqrt{\rho}} - \frac{\gamma_0}{2} \right)^D = \frac{D \gamma_0}{2} \left(\frac{a}{\sqrt{\rho}} \right)^{D-1} + o(\gamma_0 \rho^{-\frac{D-1}{2}}). \tag{81}$$

By integrating the above approximations, i.e. (79) $\sim$ (81), into (78), the whole proof is completed.

REFERENCES

[1] R. Prasad, C. R. Murthy, and B. D. Rao, "Joint channel estimation and data detection in MIMO-OFDM systems: A sparse bayesian learning approach," *IEEE Trans. Signal Process.*, vol. 63, no. 20, pp. 5369–5382, 2015.

[2] C.-K. Wen, C.-J. Wang, S. Jin, K.-K. Wong, and P. Ting, "Bayes-optimal joint channel-and-data estimation for massive MIMO with low-precision adcs," *IEEE Trans. Signal Process.*, vol. 64, no. 10, pp. 2541–2556, 2016.

[3] G. Zhu, S.-W. Ko, and K. Huang, "Inference from randomized transmissions by many backscatter sensors," *IEEE Trans. Wireless Commun.*, 2018.

[4] Darpa. Spectrum collaboration challenge (SC2). [Online]. Available: https://www.darpa.mil/program/spectrum-collaboration-challenge

[5] S. Haykin, "Cognitive radio: Brain-empowered wireless communications," *IEEE J. Sel. Areas Commun.*, vol. 23, no. 2, pp. 201–220, 2005.

[6] E. Azzouz and A. K. Nandi, *Automatic modulation recognition of communication signals*. Springer Science & Business Media, 2013.

[7] O. A. Dobre, A. Abdi, Y. Bar-Ness, and W. Su, "Survey of automatic modulation classification techniques: Classical approaches and new trends," *IET communications*, vol. 1, no. 2, pp. 137–156, 2007.

[8] B. M. Hochwald and T. L. Marzetta, "Unitary space-time modulation for multiple-antenna communications in Rayleigh flat fading," *IEEE Trans. Inf. Theory*, vol. 46, no. 2, pp. 543–564, 2000.

[9] G. Durisi, T. Koch, J. Östman, Y. Polyanskiy, and W. Yang, "Short-packet communications over multiple-antenna Rayleigh-fading channels," *IEEE Trans. Commun.*, vol. 64, no. 2, pp. 618–629, 2016.

[10] B. M. Hochwald, T. L. Marzetta, T. J. Richardson, W. Sweldens, and R. Urbanke, "Systematic design of unitary space-time constellations," *IEEE Trans. Inf. Theory*, vol. 46, no. 6, pp. 1962–1973, 2000.

[11] R. H. Gohary and T. N. Davidson, "Noncoherent MIMO communication: Grassmannian constellations and efficient detection," *IEEE Trans. Inf. Theory*, vol. 55, no. 3, pp. 1176–1205, 2009.

[12] B. L. Hughes, "Differential space-time modulation," *IEEE Trans. Inf. Theory*, vol. 46, no. 7, pp. 2567–2578, 2000.

[13] M. L. McCloud, M. Brehler, and M. K. Varanasi, "Signal design and convolutional coding for noncoherent space-time communication on the block-Rayleigh-fading channel," *IEEE Trans. Inf. Theory*, vol. 48, no. 5, pp. 1186–1194, 2002.

[14] L. Zheng and D. N. C. Tse, "Communication on the Grassmann manifold: A geometric approach to the noncoherent multiple-antenna channel," *IEEE Trans. Inf. Theory*, vol. 48, no. 2, pp. 359–383, 2002.

[15] D. J. Love, R. W. Heath, V. K. Lau, D. Gesbert, B. D. Rao, and M. Andrews, "An overview of limited feedback in wireless communication systems," *IEEE J. Sel. Areas Commun.*, vol. 26, no. 8, 2008.

[16] W. Yang, G. Durisi, and E. Riegler, "On the capacity of large-MIMO block-fading channels," *IEEE J. Sel. Areas Commun.*, vol. 31, no. 2, pp. 117–132, 2013.

[17] R. H. Gohary and H. Yanikomeroglu, "Grassmannian signalling achieves tight bounds on the ergodic high-SNR capacity of the noncoherent MIMO full-duplex relay channel," *IEEE Trans. Inf. Theory*, vol. 60, no. 5, pp. 2480–2494, 2014.

[18] W. Wei and J. M. Mendel, "Maximum-likelihood classification for digital amplitude-phase modulations," *IEEE Trans. Commun.*, vol. 48, no. 2, pp. 189–193, 2000.

[19] B. F. Beidas and C. L. Weber, "Higher-order correlation-based approach to modulation classification of digitally frequency-modulated signals," *IEEE J. Sel. Areas Commun.*, vol. 13, no. 1, pp. 89–101, 1995.

[20] A. Swami and B. M. Sadler, "Hierarchical digital modulation classification using cumulants," *IEEE Trans. Commun.*, vol. 48, no. 3, pp. 416–429, 2000.

[21] M. W. Aslam, Z. Zhu, and A. K. Nandi, "Automatic modulation classification using combination of genetic programming and KNN," *IEEE Trans. Wireless Commun.*, vol. 11, no. 8, pp. 2742–2750, 2012.

[22] N. E. West and T. O'Shea, "Deep architectures for modulation recognition," in *Dynamic Spectrum Access Networks (DySPAN), 2017 IEEE International Symposium on*. IEEE, 2017, pp. 1–6.

[23] K. Hassan, I. Dayoub, W. Hamouda, C. N. Nzeza, and M. Berbineau, "Blind digital modulation identification for spatially-correlated MIMO systems," *IEEE Trans. Wireless Commun.*, vol. 11, no. 2, pp. 683–693, 2012.

[24] P. Turaga, A. Veeraraghavan, A. Srivastava, and R. Chellappa, "Statistical computations on Grassmann and Stiefel manifolds for image and video-based recognition," *IEEE Trans. Pattern Anal. Mach. Intell.*, vol. 33, no. 11, pp. 2273–2286, 2011.

[25] C. M. Bishop, *Pattern recognition and machine learning*. springer, 2006.

[26] W. Dai, Y. Liu, and B. Rider, "Quantization bounds on Grassmann manifolds and applications to MIMO communications," *IEEE Trans. Inf. Theory*, vol. 54, no. 3, pp. 1108–1123, 2008.

[27] A. Edelman, T. A. Arias, and S. T. Smith, "The geometry of algorithms with orthogonality constraints," *SIAM journal on Matrix Analysis and Applications*, vol. 20, no. 2, pp. 303–353, 1998.

[28] J. H. Conway, R. H. Hardin, and N. J. Sloane, "Packing lines, planes, etc.: Packings in Grassmannian spaces," *Experimental mathematics*, vol. 5, no. 2, pp. 139–159, 1996.

[29] D. J. Love, R. W. Heath, and T. Strohmer, "Grassmannian beamforming for multiple-input multiple-output wireless systems," *IEEE Trans. Inf. Theory*, vol. 49, no. 10, pp. 2735–2747, 2003.

[30] L. Xu and M. I. Jordan, "On convergence properties of the EM algorithm for Gaussian mixtures," *Neural computation*, vol. 8, no. 1, pp. 129–151, 1996.

[31] H. Karcher, "Riemannian center of mass and mollifier smoothing," *Communications on pure and applied mathematics*, vol. 30, no. 5, pp. 509–541, 1977.

[32] P.-A. Absil, R. Mahony, and R. Sepulchre, *Optimization algorithms on matrix manifolds*. Princeton University Press, 2009.

[33] Y. Chikuse, *Statistics on special manifolds*. Springer Science & Business Media, 2012, vol. 174.

[34] R. Tarjan, "Depth-first search and linear graph algorithms," *SIAM journal on computing*, vol. 1, no. 2, pp. 146–160, 1972.

[35] A. Barg and D. Y. Nogin, "Bounds on packings of spheres in the Grassmann manifold," *IEEE Trans. Inf. Theory*, vol. 48, no. 9, pp. 2450–2454, 2002.

[36] P. Gupta and P. R. Kumar, "Critical power for asymptotic connectivity in wireless networks," in *Stochastic analysis, control, optimization and applications*. Springer, 1999, pp. 547–566.